POLITECNICO MILANO 1863

SCUOLA DI INGEGNERIA INDUSTRIALE E DELL'INFORMAZIONE

# Experimental Investigation of Tandem Propeller Aeroacoustics in Hover Condition

Tesi di Laurea Magistrale in Aeronautical Engineering - Ingegneria aeronautica

Author: **Ilaria Savoldi**

Student ID: 990133
Advisor: Prof. Alex Zanotti
Co-advisors: Donato Grassi, Luca Riccobene
Academic Year: 2022-23

# Abstract

The objective of this research is to understand the mutual influence of two propellers in a hovering state, varying their tip-to-tip distance and the disk-to-disk distance. The different configurations were studied throughout an experimental investigation conducted in a completely anechoic chamber. Acoustic data were collected using an array of 12 microphones arranged in a circle on the plane containing the propellers rotational axes. The result is that the performances slightly reduce with the propellers getting closer with a disk-to-disk distance fixed, and are not significantly affected by changing the distance between the disks. Indeed when the propeller blades overlap, the performances actually decrease. The aeroacoustic performances show an analogous trend, without overlapping, the generated noise is more or less the same for different tip-to-tip distance. However, as soon as the wake of the forward propeller interacts with the blades of the other propeller, in the staggered cases, the noise generation increases. The increase affects both the tonal and broadband components of the noise; in particular, the OASPL can increase by as much as $15dB$ from the farthest to the closest configuration. The enhancement in tonal peaks is due to the increasing thrust fluctuations, which translate into an increase in the loading noise. On the other hand, the increase in the broadband component is due to the presence of more vortexes since when there is overlapping, there is an increase in the TKE. Moreover, it was found that the co-rotating propellers perform better than the counter-rotating ones when they are close enough to each other and vice versa when they are far enough apart.

**Keywords:** Aeroacoustics, eVTOL, propeller, hover

# Abstract in lingua italiana

Questo studio ha come obbiettivo comprendere l'influenza che due propeller esercitano l'uno sull'altro al variare della distanza tra la punta e tra i dischi di rotazione delle pale. Le diverse configurazioni sono state studiate sperimentalmente in una camera completamente anecoica. I dati riguardanti l'acustica sono stati acquisiti tramite 12 microfoni posizionati in cerchio attorno ai propeller sul piano contenente l'asse di rotazione dei medesimi. Si è analizzato che le prestazioni si riducono man mano che i propeller vengono avvicinati lateralmente a distanza tra i dischi fissata, mentre un cambiamento in quest'ultimo valore non è rilevante. Le prestazioni vengono però notevolmente ridotte quando c'è sovrapposizione dei dischi siccome il propeller retrostante è catturato all'interno della scia dell'altro. Le prestazioni acustiche hanno a loro volta un trend analogo siccome senza sovrapposizione il rumore prodotto è all'incirca costante al variare della distanza relativa. Invece appena c'è sovrapposizione, nei casi in cui il valore della distanza tra i dischi non è nullo, il propeller retrostante interagisce con la scia dell'altro e l'impronta sonora registrata è nettamente superiore. L'aumento di intensità sonora è registrato sia nella parte tonale che nella parte a banda larga, in particolare il valore di OASPL aumenta fino a $15dB$ dalla configurazione con i propeller più lontani a quella di massima sovrapposizione. I picchi tonali aumentano a causa dell'aumento di fluttuazioni della spinta che si concretizzano in un aumento di rumore si loading. L'aumento nella componente di broadband è invece dovuto alla presenza più intensa di vortici, poichè, dove c'è sovrapposizione, si registra un aumento di TKE. Inoltre è stato constatato che che le configurazioni con i propeller corotanti sono più performanti delle controrotanti per basse distanze ed il trend si inverte nel caso di distanze maggiori.

**Parole chiave:** aeroacustica, eVTOL, propeller, decollo verticale

# Contents

# Introduction

The need to reduce carbon dioxide emissions is strongly felt nowadays, and one of the main goals of transportation engineering is to achieve both environmentally friendly land and air mobility. In addition, urban traffic is increasing, making ground transportation less efficient, especially in large cities. One solution that would be both environmentally sustainable and avoid road traffic is the use of the eVTOL: electric vertical take off and landing, a fully electric rotor-craft. Rotor-crafts are not an innovative way of flying, as they have always been used in military and civil aviation, but the main problem is that they can only carry people and goods at low flight volumes and, moreover, their acceptance in urban areas is limited by their noise generation.
The structure of an eVTOL differs from that of a conventional rotor-craft because it has a multi-rotor structure with rigid blades that do not allow pitching motion (as would be the case with a conventional helicopter) and only allow rotation as a degree of freedom. In addition, the eVTOL can take off and land vertically like a conventional helicopter to fly more easily between massive buildings, and, above a certain altitude, it can gradually tilt its rotors horizontally to convert into a configuration of forward flight working more similarly to an airplane.

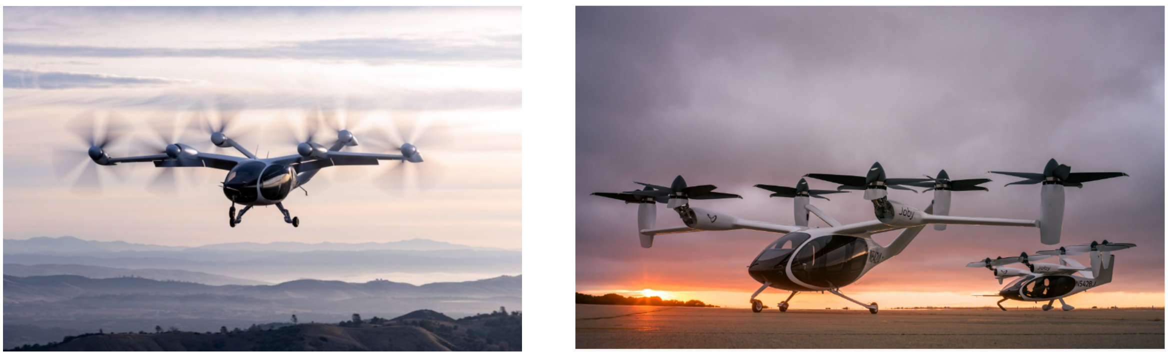

(a) eVTOL of Joby aircraft in forward flight configuration.

(b) eVTOL of Joby aircraft in take off and landing configuration.

Figure 1: Joby aircraft eVTOLs.

In this configuration, unlike conventional helicopters, eVTOLs exploit the rotors to generate thrust rather than lift to propel the rotor-craft forward. Consequently, the blades are subjected to less load than in the takeoff and landing phase, and the RPM (revolutions per minute) can be reduced in line with energy consumption, since part of the load is transferred to the wing structure.

The eVTOLs will prove useful when there is a need to bypass ground transportation, as they are able to fly over traffic to expedite the movement of people and goods. The benefits that these vehicles could bring have already been recognized by various companies, and many of them have already decided to invest in the eVTOL sector. For example, in the near future, the airline United Airlines will launch a project at Chicago and Newark airports, whose goal is to transport people from the airport to the city center and vice-versa in the shortest possible time ($10-20$ minutes), taking advantage of the capabilities of eVTOLs.


Figure 2: United Airlines eVTOL.

Investments in the eVTOL sector have been made not only in the aircraft itself, but also in the related infrastructures. In Coventry, the UK government and Hyundai have invested in a dedicated hub. This infrastructure was built to occupy the smallest possible space, in fact its dimensions are 60% smaller than those of a normal airport. The intention is to build many more airports of this type all over the UK in the near future. These are just a few examples of the investments that have been made in the eVTOL sector, but they are not the only ones, as many other companies have recognised the possibilities of eVTOLs and have done the same.


Figure 3: EVTOLs hub at Coventry.

Even though these new aircrafts would help to reduce carbon dioxide emissions, they would cause another type of pollution, noise pollution. Noise is a major barrier to public acceptance, it is possible to understand that just thinking about the complaints of people who live near regular airports. So eVTOLs need to be quiet enough to fly in an urban context and also be accepted by the public and certifications. Electric engines are much quieter than conventional internal combustion engines, but the aircraft produces much aerodynamically-generated noise from the rotating blades. Noise generation may also come from possible unsteady aerodynamic interaction between the various components of the eVTOL: Rotors, propellers and fixed aerodynamic surfaces.

Another disadvantage is the fact that an electric motor weighs much more than a standard motor and has lower capability, so the transport of payload would be limited in terms of quantity and range. A description of different types and configurations of eVTOLs is given by Erick Greenwood [7]. This article also proposes possible active and passive mechanisms to reduce noise generation.

# 1 | Chapter One
# State of the Art

The eVTOL has all the prerequisites to become the urban people and freight transport of the future, but excessive noise generation remains one of the biggest problems that must be solved to allow this rotor-craft to fly without bothering much the human hearing. Knowing how attractive this rotor-craft could be for urban mobility thanks to the advantages mentioned above, it is important to develop experimental and computational tools to analyse and reduce noise generation in order to make the eVTOL acceptable to the public. Since one of its peculiar characteristics is the presence of a series of rotors, both rotor-to-rotor interaction and single rotor characterization have been topics to many researches.

In the following section some of the main results that have been achieved on this subject both from the experimental and numerical point of view are highlighted. The novelty of this research is to investigate how the variation of the relative distance between two propellers affects their aeroacoustic and aerodynamic performance through an experimental approach, in particular taking into account the overlapping of the propellers.

Some experiments have already been performed on isolated propellers to investigate both their acoustic and aerodynamic performance. In particular, Zawodny et al. NASA [13] have tested two different model rotors from both numerical and experimental points of view. The aeroacoustics was well investigated using several instruments that are the same that have been used in this work, as shown in the results section. In particular sound pressure level analysis, power spectral density analysis, broadband interpolation and a weighting filter were used. They were also able to simulate their case using high-fidelity methods and obtained good agreement with the experimental results. Moreover, they discovered that between the two configurations there is a difference both in noise level production (up to $8dB$) and directivity even if they are under the same thrust condition, figure 1.1. This difference is mainly attributed to the different wing tip speed.

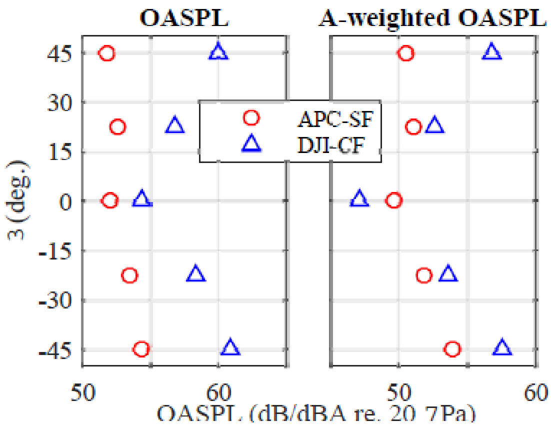


Figure 1.1: Difference in the noise production of the two propellers (plots taken from[13]).

They discovered that recirculation has a certain impact on rotor noise. Recirculation affects much the experimental analysis in a closed anechoic chamber since the flow develops influencing both thrust and acoustic signal enhancing both tonal and broadband noise. This discovery reduces the window of time in which is possible to collect experimental data before being influenced by the recirculation effect and so the additional flow that would be present in regime condition. Measurements should not be taken carelessly without considering the effect of recirculation after the rotor is stabilised.
It is also important to remember that, since the eVTOLs are multi rotor bodies, the aerodynamic and acoustic interaction between different rotors is inevitable and has an impact on the design of the rotor-craft.

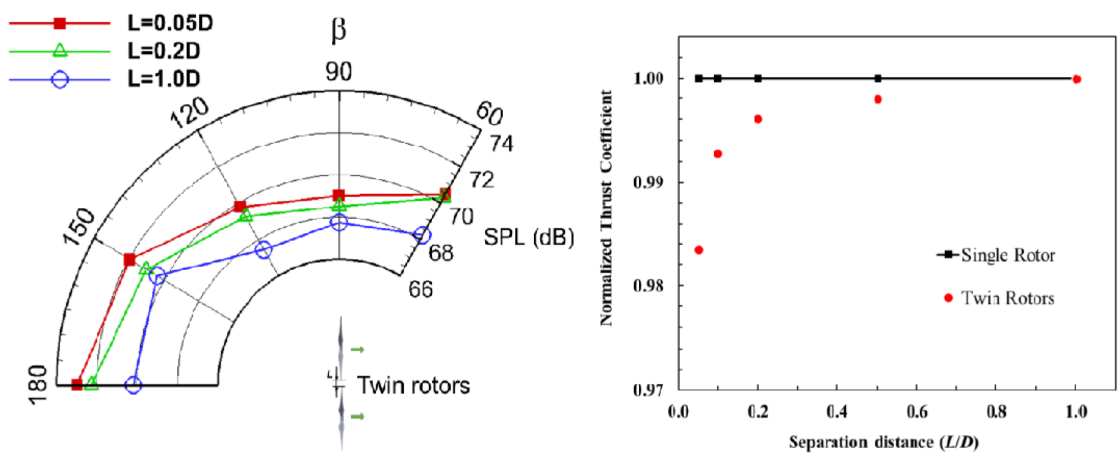


Figure 1.2: Normalised thrust behaviour and OASPL behaviour varying the angle (plots taken from [14]).

Twin propeller configuration was indeed studied by Wenwu Zhou and his team [14] but they limited themselves to analyse the influence of relative distance without varying the separation along the $y$ axis (the distance between the axes of rotation can vary but not the distance between the planes of rotation of the two propellers). With this analysis it is possible to see the influence of the distance but, with $dy/r = 0$, there is no overlapping of the two blades disk that, as it is intuitive, can have a huge effect since the back propeller would be caught in the wake of the other one. In this study they obtained that the distance for which the two propellers are not considered to influence one another is one time the diameter, while for closer distance they gradually lose thrust and increase noise production, this increase in noise, in both tonal and broadband parts, is attributed to the increase of turbulence in the wake and to the increasing thrust fluctuations, as also T. Carolus affirms [5]. They also observed that the SPL has a specific behaviour since it is monotonously increasing from the side to the front of the propeller, figure 1.2.

A twin propeller configuration was also studied by Austin David Thai and his group [10], both from numerical and experimental point of view. They observed that the interaction, in the twin propeller configuration always reduces the performances with respect to the isolated case, resulting in a lower thrust and a higher torque. Both the performance parameters reach the ideal value of the isolated propeller when they are far enough. Moreover, the sensitivity of the parameters to the interaction is different since the thrust varies in average of 1% while the torque of $0,5\%$ with respect to the isolated case. These differences may not have an impact on a real propeller influenced by an external environment indeed. Also, the counter-rotating case was tested and they observed that, because of a higher number of interactions the thrust is reduced and the torque is increased, figure 1.3 Moreover, the counter-rotating configuration also seems to generate higher noise (around $1dB$ higher).

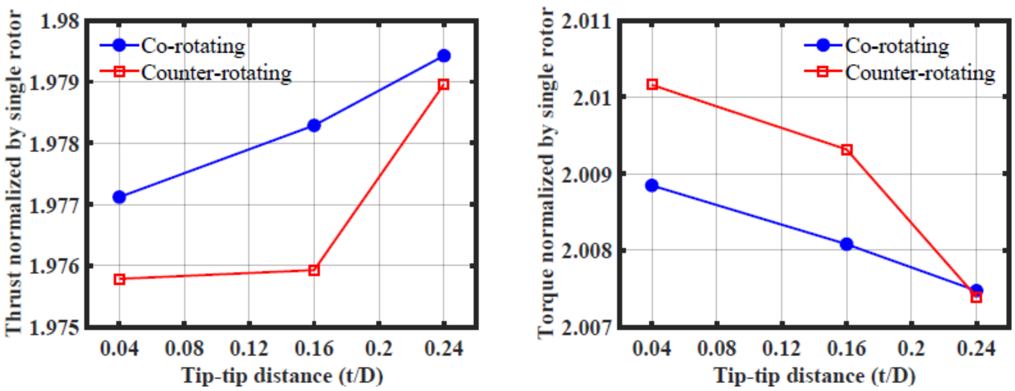


Figure 1.3: Normalised thrust behaviour and torque varying the distance between the two propellers (plots taken from[10]).

In the recent years some solutions were also suggested to apply on the rotor to reduce the noise production, passive devices became of interest since they do not require power to work but can still bring some improvement to performances and noise production. In particular serrated edges were suggested by Yang et al. [12]. The serration of the edge is inspired by the wings of the birds and on an eVTOL blade it can be reproduced varying different parameters. Propellers with this modification, in particular an add-on serration, have a higher efficiency from the aerodynamic point of view with respect to a standard rotor working at the same rpm, while the opposite goes for cut-in serration. Throughout an OASPL analysis they discovered that in general serrate edge propellers produce lower noise both in broadband and tonal component than the baseline propellers. They also did some PIV (particle image velocimetry) experiments to better understand the physics behind the phenomenon.

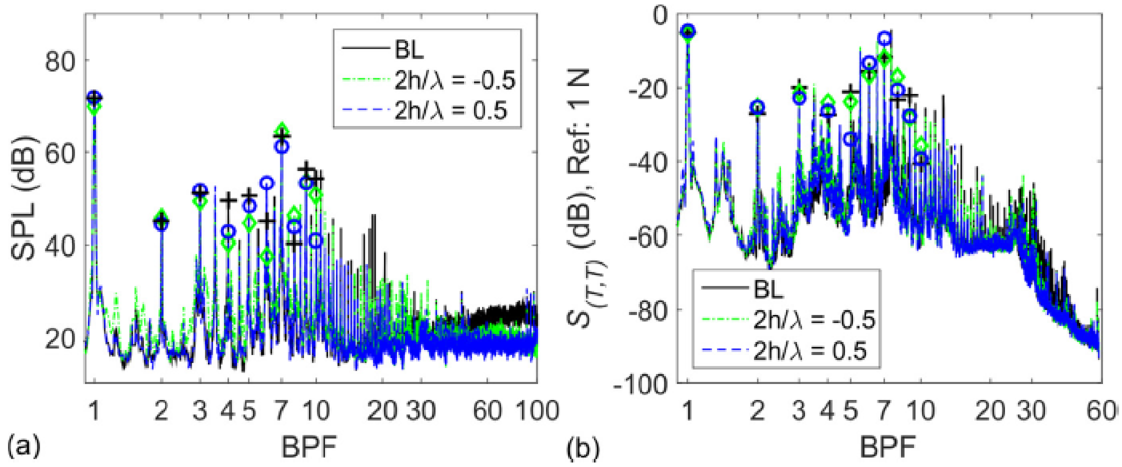


Figure 1.4: Comparison between PSD of serrated blades (plots taken from[12]).

In figure1.4, are shown the PSDs obtained for different cases where BL stands for base line propeller, and the parameters $h$ and $\lambda$ and respectively half of the serration height and the wave-length of serrations.

Alvarez and his team [4] used two different numerical methods to test the mutual influence of two propellers varying the tip-to-tip distance. Once more the separation along $y$ axis was kept fixed to zero while the distance between the two rotational axes was varied. In this research, two different methods were used, the first one is a classical CFD mesh-based method that exploits the URANS, while the second is based on a Lagrangian solver and uses a mesh-less VPM method (vortex particle method). This second method exploits principles that get very close to DUST[1]. The parametric study of rotor-to-rotor interaction was done on the hover condition on a two blade propeller. They observed that the performances drop when the propellers get closer and moreover the largest thrust fluctuations (And potentially highest noise signature) are registered at the lowest distances, figure1.5.

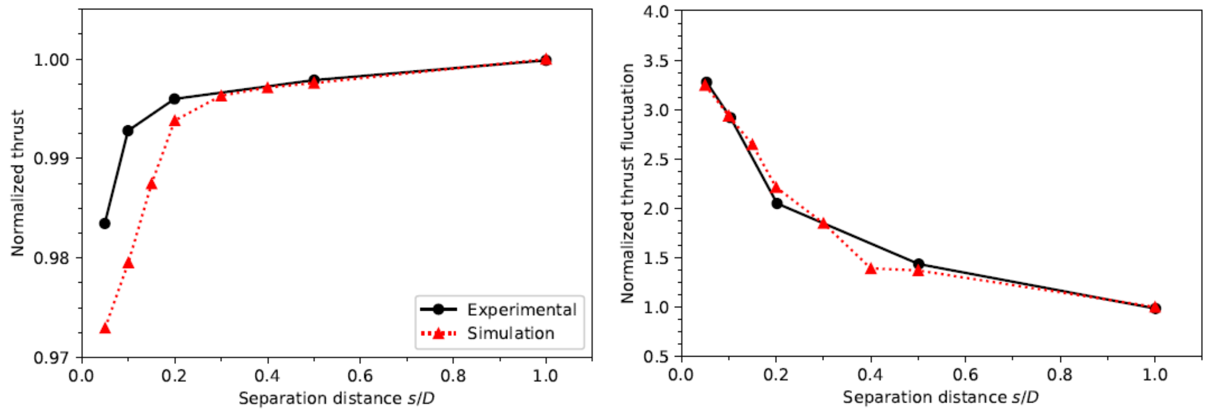


Figure 1.5: Normalised thrust and normalised thrust fluctuations behaviour (plots taken from [4]).

Beside the variation of the relative distance between the two propellers, other elements influence the aeroacoustics of the performances. As Russell says [9] the material of which the blades are made can influence their deflection and so their performance. Injection plastic molded blades are easier to deform and so they can induce vibration. Nevertheless aeroelastic simulations of the propellers show a better agreement with the measurement data. Also Piccini and his crew analysed twin propellers configuration [8]. In particular, they analysed, through the numerical mid-fidelity tool DUST, the performances of side by side propellers and tandem propellers. They obtained that once the propellers are in tandem configuration their performances are drastically reduced, this derives from the fact that the back propeller is caught in the wake of the other one. DUST is a powerful mid-fidelity numerical tool, since it allows to easily and rapidly simulate difficult scenarios. In particular it comes in handy when dealing with non-stationary cases and propellers. With a CFD high-fidelity method the mesh should, at each instant of time, adapt to the new configuration of the blade, but with a particle method like DUST this adaptation is no longer required. DUST's development contribution and application to eVTOLs can partially be attributed to Tugnoli that explains his results [11]. Moreover, DUST has been coupled to $SU^2$[2] to permit the study of the acoustics. It is important to cite also Algarotti's work [3] since he did particle image velocimetry and numerical simulations with DUST on the same model propellers used for this research, but in forward flight conditions instead.

## Motivations

The aforementioned studies, in case of tandem configuration, analyse the propellers mutual interaction varying the relative distance between the two axes of rotation. Instead the variation of the distance between the two planes of rotation is not considered. This research aims to confirm the previously achieved results in case of $dy/r = 0$ and also add an analysis with a variation of the separation along $y$ axis value giving a more detailed analysis of the influence of the distance between two propeller mounted on an eVTOL aircraft. Moreover, when $dy/r$ is different from zero, the propellers can be brought closer and the planes of rotation can overlap allowing the generation of different phenomena making the physics to strongly differ from the not staggered case. The staggered configurations with the overlap of the planes of rotation can therefore be considered as a case that stays between the completely coaxial tandem propellers configuration and the side by side configuration. This case has never been investigated and still needs to be studied and understood. The staggered configurations, as a matter of fact, should differ from the ones with $dy/r = 0$ both from performance and aeroacoustic point of view.

Many models of eVTOLs have already been realised and are ready to fly, but one of the main obstacles is to pass the certifications required in terms of noise emission. The topic of this thesis is therefore to illustrate, throughout the experiments conducted in an anechoic chamber, how the production of noise of a twin propeller configuration differs varying the relative distance between two rotors moving them both on $x$ and $y$ axes, the two coordinates are on the plane containing the axis of rotation. Since the eVTOLs need to be certified to fly the main aim of this research is to find the best configuration concerning the $dy/r$ value and mutual tip-to-tip distance for two rotors, or at least it aims to find the worst ones to avoid. Also the aerodynamic forces were studied throughout load cells to understand their behaviour since, as it was already stated, the acoustics is not the only element influenced by the mutual distance of the propeller and the best configuration that should be adopted in an eVTOL is the one that guarantees the best performances and the lowest noise emission.

# 2 | Chapter two Experimental Setup

In this chapter, both the experimental setup and the test matrix are described. In particular, the anechoic chamber will be presented first, followed by the description of the propeller, the electronic instrumentation, the test matrix and in the end the different configurations tested will be shown.

### 2.0.1. Anechoic Chamber

The anechoic chamber's dimensions, considering just the available space without the cones, are $4x4x4m$. The walls and ceiling are covered by Phono-absorbent panels which demolish short length acoustic waves and phono-absorbent big spires made of polyester wool (the height is $700mm$, which reduces the actual available space) which cut off the long wavelength of the acoustic signal, figure 2.1. The aim of testing a propeller inside an anechoic chamber is to avoid the reflection on the walls, ceiling and floor of the acoustic waves that would alter the measurements, this is possible since the waves are absorbed by the spires and the panels. As a matter of fact measuring inside an anechoic chamber is the same as measuring in a completely free environment. Every anechoic chamber is characterised by a cutoff frequency that is the point in the frequency regime where the registered signal is attenuated or blocked, in this case it corresponds to $f_{CUT} = 150Hz$. The chamber allows both the semi-anechoic configuration and the completely anechoic configuration since the panels and the spires on the floor are removable. The configuration adopted in this case was the one of completely anechoic chamber.

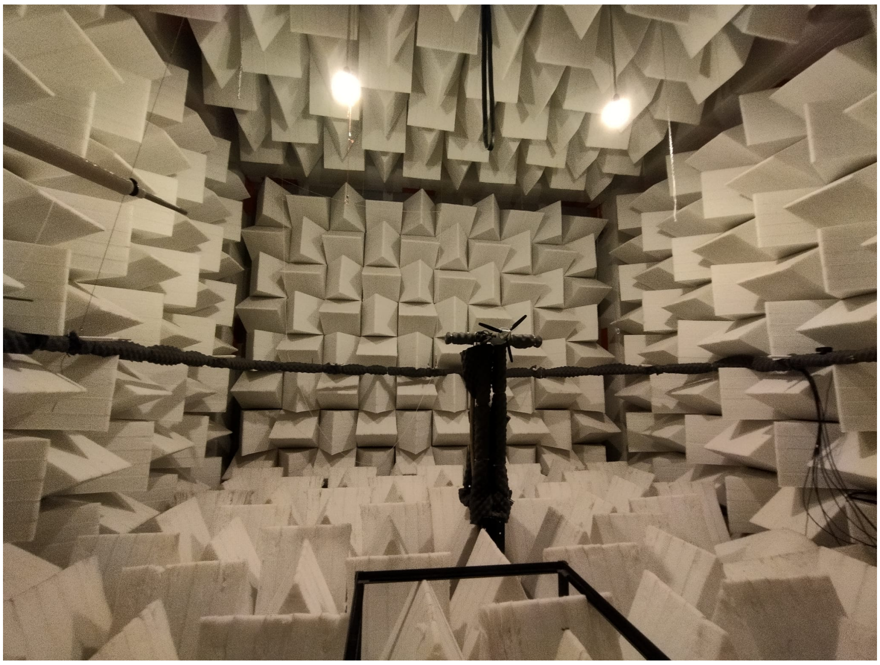

Figure 2.1: Anechoic chamber of the energetic department of Politecnico of Milan.

### 2.0.2. Propellers description

In the present research both single and tandem propellers configuration were studied so two propellers were needed. In particular two identical model propellers were chosen. These two models are the same ones that were used in a previous work thesis "Experimental-Numerical Investigation of the Aerodynamic Interaction between Tandem Propellers in eVTOL Airplane Mode" from Algarotti 2020-2021 [3] as a matter of fact some of the instrumentation used coincides with the one used for this previous work. The models are 3-blade propellers, in particular VarioPropeller 12C. The blades are easily removable and can be changed between right and left handed with the inversion of the verse of rotation. The nominal diameter of the blades is $300mm$, while the spinner is $65mm$. The angle of attack of the blades is set by a mechanical mechanism that imposed them to have the same value assuring symmetric conditions. The roots of the blades are fixed in an aluminum hub which is mounted on the propeller shaft and fixed through a bolt on an endless screw, on which, in turn, the cover is mounted of the hub. Everything is fixed together to avoid relative motion. Globally both the geometry and the structure get very close to the ones of a real eVTOL. Throughout a system of washers the pitch was fixed for all the blades to be $\alpha = 15°$, the pitch chosen has this value in order to be as close as possible to an eVTOL full scale in hover condition, moreover a bigger pitch would have implied more noise and bigger separation areas. The power comes from a Scorpion HKII-4235-630KV brush-less electrical motor, figure 2.2a, this is also equipped with a

Hall effect sensor, that, giving as output a signal for each rotation, allows to instantly read the RPM. The driving system is a Hobbywing Platinum V4 (120A) ESC, figure 2.2b, which is able to control the power input as a real rotor. The driving system was placed outside the nacelle, in particular on the holding structure.
The power supply system provides constant current at $5kW$. Since this object is massive and also, while working, produces a lot of noise, it was placed outside the chamber and connected to the driving system with a system of wires to limit the disturbance on the tests.
A Labview software was suitably designed for the tests, with this it is possible to remotely control the power supplied to the motors, and consequently the RPM. The Labview software is also responsible for the acquisition of both performance and acoustic data. The load cells, the load sensor and the propulsive system are all contained in an aluminum nacelle.

The outside view of the model is visible in figures 2.2c and 2.2d, while the internal structure from figures 2.2e and 2.2f where it is possible to see that the propeller is made by three separated compartments:

- On the left there is the slot for the balance sensor placed in order to avoid any unwanted contact with the structure.
- On its right there are the four balance columns to directly connect the blades and the sensor. Since the contact with other structure is unwanted there is a void between the cage and the motor.
- In a similar way, at the far right the hub is positioned and is connected to the motor throughout a shaft.


(a) Scorpion HKII-4235-630KV brush-less electrical motor.


(b) Hobbywing Platinum V4 (120A) ESC driving system.

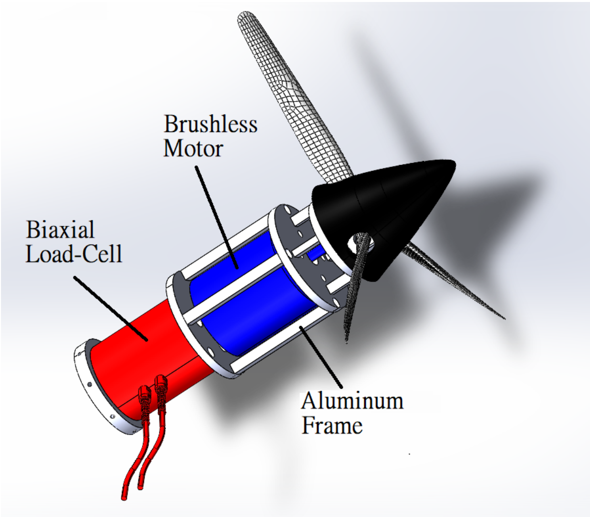


(c) Visualization of the internal components of the propeller.

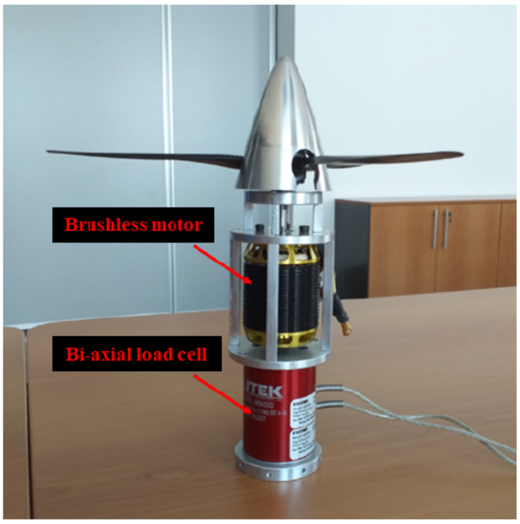


(d) Photo of the internal component of the propeller.

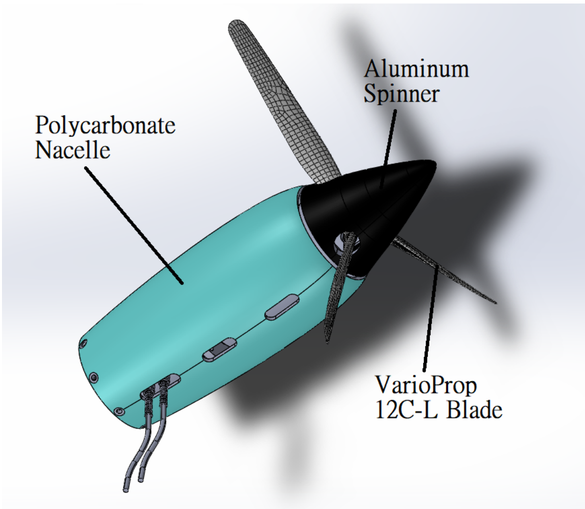


(e) Visualization of the external view of the propeller.

(f) Photo of the external view of the propeller.

Figure 2.2: Propeller and its components.

### 2.0.3. Propeller Setup

It was decided to test the propeller horizontally, in order to not have the ground effect that the presence of the floor would give, placing the propeller accordingly the wake has more space to propagate, moreover it is easier to place the microphones on the plane of interest (the one containing the axes of rotation). Studying the acoustic on the plane containing the blades would be less interesting since a symmetric behaviour at different angle is expected. The structure to hold the propellers was realized adjoining Bosch© profiles of different dimension adding upwind supports to make the structure less flexible and deformable to the forces applied, figure2.3. To test different relative tip-to-tip distances, the propellers could slide along the side of the profile and then they could be fixed with screws and bolts. To add a separation along $y$ axis another Bosch© profile had to be added in particular a chock of $75mm$ in case of $dy = 1r$ and one of $32,5mm$ in case of $dy = 0,5r$. The structure was fixed to the floor, at the center of the chamber, throughout an iron robust structure. Finally the whole structure was covered with phono-absorbent material to avoid acoustic reflection.

Figure 2.3: Bosch© structure on which a single propeller is mounted.

The microphones to be arranged were twelve and had to be positioned equally spaced around a circle, in particular they were positioned at 30° spacing between one another with the first starting directly in front of the propeller. Since the acoustics needs to be tested in the farfield the microphones were placed as far as possible from the propellers, in particular they were placed on a circle of ray $1800mm$ (figure 2.5), this correspond to 12 times the ray of the blades. The diameter of the circle of the microphones is smaller than the distance between the walls since the actual space available is reduced by the spires whose height is $700mm$. Also, microphones needed a structure to be held and this was made in wood to weigh less and be hung from the ceiling. To make it easier to be realised the structure was not a circle, as it is more intuitive, but a hexagon, on each side two microphones were placed. The structure was hung from the ceiling and fixed to the walls so that it was not allowed to oscillate interacting with the wake. The height at which the structure was fixed was $165cm$ that is the same height at which the axes of rotation are. In this way the reading of the microphones is done exactly on the same plain of the rotational axes. Moreover, the microphones were not placed directly on the wood structure but on some 3D printed holders to create some space between them and the structure, the aim of this was to reduce as much as possible the interference in the acquired pressure fluctuations. Since the microphones did not have all the same shape these 3D printed holders had different length to allow all the microphones to read the fluctuations at the same distance from the centre of the chamber, figure 2.4a and 2.4b.

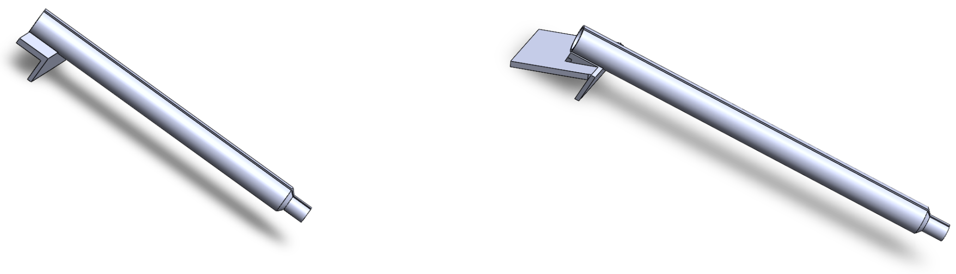

(a) Structure holding the microphones of the first kind.

(b) Structure holding the microphones of the second kind.

Figure 2.4: Structures holding the microphones.

After placing everything in position and connected the different wires, both the structure to hold the microphones and the one for the propellers were covered by phono-absorbent material to not reflect the acoustic waves and interfere with the measurements. Figure 2.5 show a scheme of the experimental setup arrangement.

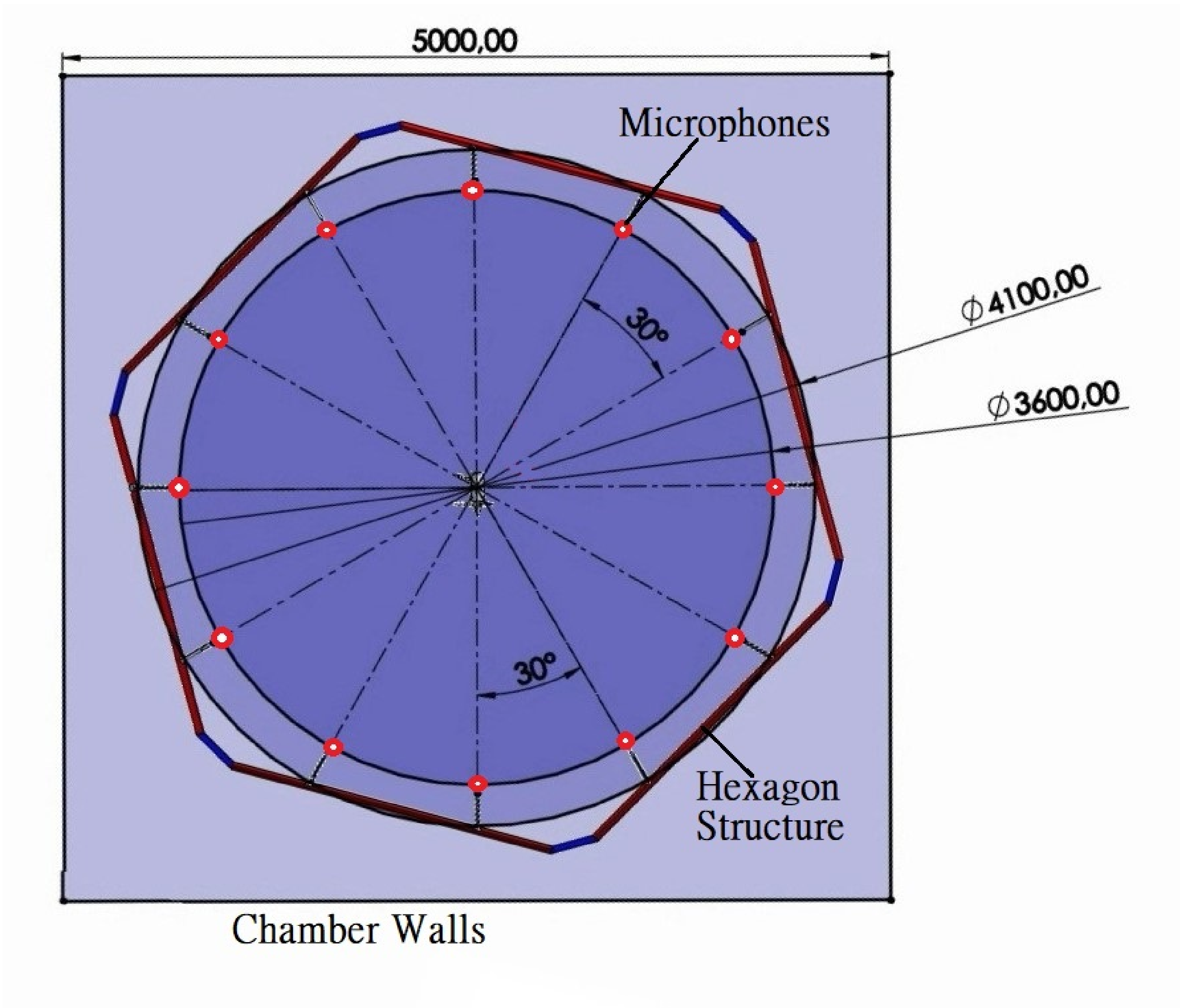


Figure 2.5: Scheme of the placement of the microphones with a representation of the propeller in the middle.

The chamber allows both tests in a completely anechoic configuration and in a semi-anechoic configuration since the floor is removable, the intention was to conduct the experiment in a completely undisturbed environment so the completely anechoic chamber was opted for, figure 2.6.

Figure 2.6: View of the anechoic chamber in a completely anechoic setup.

### 2.0.4. Loads Measurements Setup

The balances used are inner balances and they are placed inside each nacelle, the two items make it possible to instantaneously read the output of two separate loads, in particular the thrust, the axial force produced, and the torque, the couple of forces exerted on the propellers axes. The cells are composed by a FUTEK MBA500 strain gauge bi-axial load cell (50 lbs F.S.), figure 2.7. Since the space inside the nacelle is limited, the choice was a compact sensor. The calibration of the sensors was done previously by Algarotti, and the data that were obtained are reported in table 2.1. Throughout test high linearity performances were confirmed. At the bottom of the nacelle the load cells have a dedicated slot, while the active end is fixed at its root, it is also facing the plate that throughout columns is connected directly to the hub to allow the loads to be transferred from the blades. The only loads that the cells can read are the ones coming from the blades since the cylindrical non-loading surface is carefully placed inside the nacelle avoiding any kind of contact that would interfere with the measurement. As a matter of fact, also the cables that carry the data outside the nacelle pass throughout a hole without touching the walls. The Labview software that was already mentioned to control the RPM also allows to read the forces. A cycle was designed in which the time to get to regime was fixed at $8s$ (this was measured before starting the tests), to have measures stable in time, moreover the duration of the measurement was fixed at $10s$. The sample frequency is $25000Hz$. Every time that the cycle starts the system sets to zero the forces acquired in order not to have any kind of bias and make the measurements more repeatable. Through wire the balance sensors are connected to a module that allows to read the data output, the module is an analog module NI-9237 by National Instruments that, in turn, is connected to a CompactDAQ device.

| | |
|---|---|
| Performance | |
| Non-linearity | +-0.25% of RO |
| Hysteresis | +-0.25% of RO |
| Non-repeatability | +-0.25% of RO |
| Mechanical | |
| Safe Overload | 150% of RO |

Table 2.1: Cell sensor characteristics.

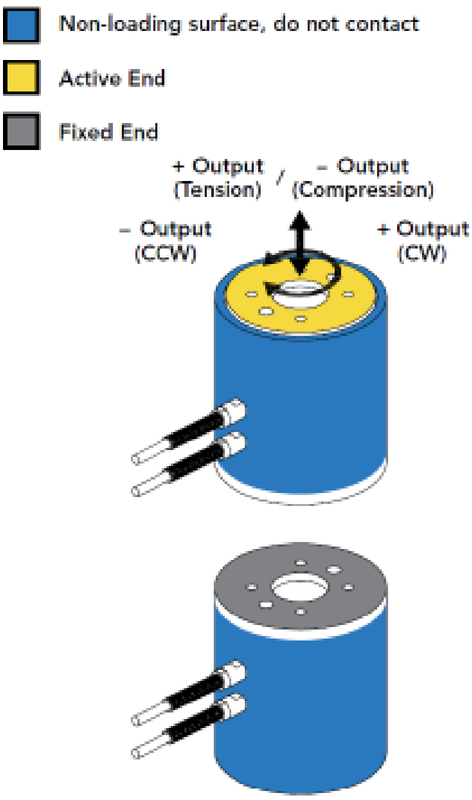


Figure 2.7: FUTEK MBA500 strain gauge bi-axial load cell (50 lbs F.S.)

### 2.0.5. Microphones

12 microphones were chosen and connected to a module in order to be read. All the microphones responses in frequency were checked before thanks to a piston-phone. A piston-phone is a handheld tool to check frequency microphone response, in particular it produces pressure fluctuations of known frequency. The working principle is based on a vibrating piston that compresses a fixed volume of air on whose other side it is exposed to a diaphragm that starts vibrating in turn [6] page 248. The microphones responses were therefore evaluated first at frequency $1000Hz$ and, since the amplitude of the output signal is known, their sensitivity was obtained, then they were tested at different fixed higher and lower frequencies. The responses of the microphones at different frequencies are reported in Appendix A.

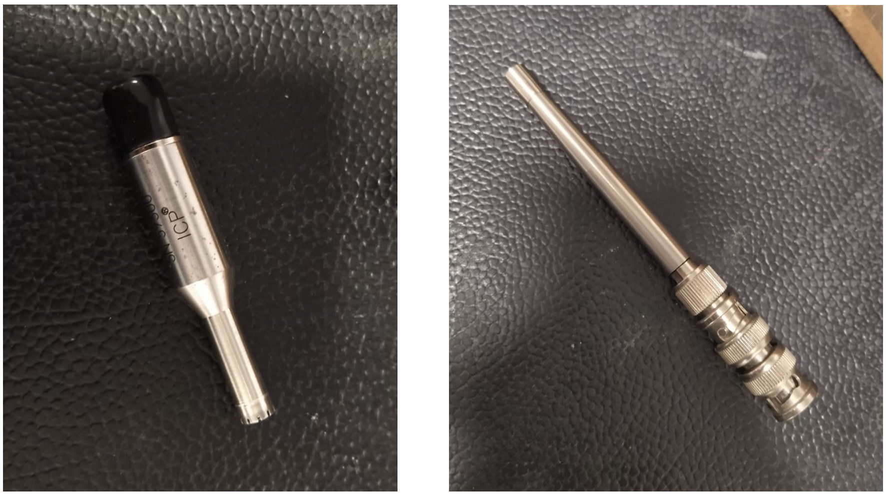

(a) Microphone of the first kind. (b) Microphone of the second kind.

Figure 2.8: Different type of microphones used.

The microphones used were of different kind due to the availability of the instrumentation:

- 10 ROGA microphones, figure 2.8b
- 2 PCB microphones, figure 2.8a

### 2.0.6. Test Matrix

In the following section the different configurations that were tested are going to be presented. The configuration to be studied was the hover condition, this means in vertical take off or landing condition without the presence of an axial flow. In particular, in this configuration, the analysis of the effect on performance and on noise production of the relative distance between the two propellers and the $dy/r$ value became of interest. Relative tip-to-tip distance means the distance along $x$ axis between the two blade tips. In a staggered configuration, instead, there is a forward displacement so the distance between the two planes of rotation of the blades is not null.

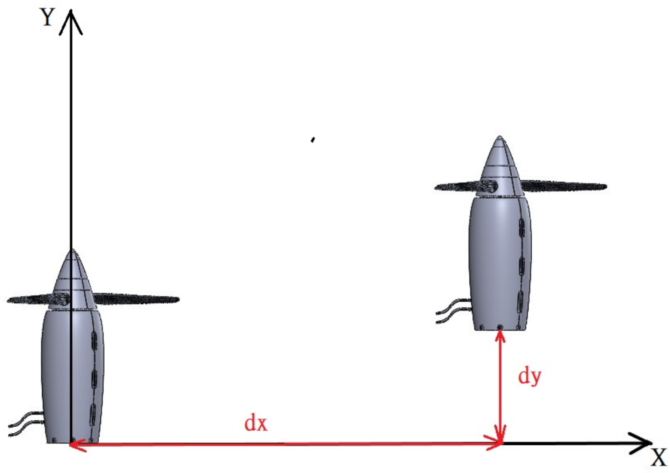


Figure 2.9: Illustrative image of the twin propeller set up, on $x$ axis there is the relative distance and on $y$ axis.

First of all, the isolated propeller configurations were studied, in this case the second propeller was removed from the chamber. The propeller was characterised both from the performance and acoustic point of view.

In case of $dy = 0r$ several relative distances were tested: $1r$, $0,5r$, $0,25r$, $0,1r$. These distances are measured from the tip of the blades of one propeller to the other one. The propellers were both co-rotating clockwise, but these same distances were repeated in case of them counter-rotating, in particular the blades of the second propeller (the one added after the isolated propeller tests) were changed with left-handed blade, in order to have the same thrust direction and sign of the first one even if counter-rotating. The distance of $1r$ is meant to simulate a condition in which the propellers are far enough to not influence each other.

In case of $dy = 0,5r$ these relative distances were tested: $1r$, $0,5r$, $0,25r$, $0r$, $-0,25r$, $-0,5r$. This time the rotating blades could overlap, this overlapping was done in a measure to prevent the tip of the blades of the back propeller to touch the nacelle of the other one. All the distances were also tested with the two propellers counter-rotating.

Another case of $dy = 1r$ was tested to analyse what was the impact of varying the $dy/r$ distance between the propellers. All the configurations tested are reported in the test

| | | $dy/r$ | | |
|---|---|---|---|---|
| | | 1r | 0,5r | 0r |
| dx/r | 1r | Co-rotating | Co/Counter-rotating | Co/Counter-rotating |
| | 0,5r | Co-rotating | Co/Counter-rotating | Co/Counter-rotating |
| | 0,25r | // | Co/Counter-rotating | Co/Counter-rotating |
| | 0,1r | // | // | Co/Counter-rotating |
| | 0r | Co-rotating | Co/Counter-rotating | // |
| | -0,25r | // | Co/Counter-rotating | // |
| | -0,5r | Co-rotating | Co/Counter-rotating | // |

Table 2.2: Table representing the different tested configurations

| RPM | Reynolds | Ma |
|---|---|---|
| 6000 | 194000 | 0,27 |
| 7000 | 226000 | 0,32 |
| 8000 | 259000 | 0,37 |
| 9000 | 291000 | 0,41 |

Table 2.3: Table reporting the tests data.

matrix 2.2. Moreover, the noise of the motor in both isolated and tandem configuration was tested. These tests were done removing the hubs and the blades from the structure. Each $dx/r$ and $dy/r$ distances were tested for different RPM in particular: $6000rpm$, $7000RPM$, $8000RPM$ and $9000RPM$. In table 2.3 the respective tip Reynolds and Mach number are also reported. Moreover, every configuration test was repeated three times in order to improve the repeatability and accuracy of both the performance ad acoustic results.

# 3 | Chapter three

# Experimental Results

The experimental results are divided into two paragraphs. In the first one the results concerning the aerodynamic performance are going to be shown, thrust coefficient and thrust fluctuations. In the second paragraph there are going to be results concerning an aeroacuostic analysis, in this case the analysis is going to focus on power spectral density, sound pressure level analysis, broadband interpolation and A weight filtering.

### 3.0.1. Propeller performance

In this subsection the performances of both the isolated propeller and the tandem propellers configurations are shown and compared to each other.

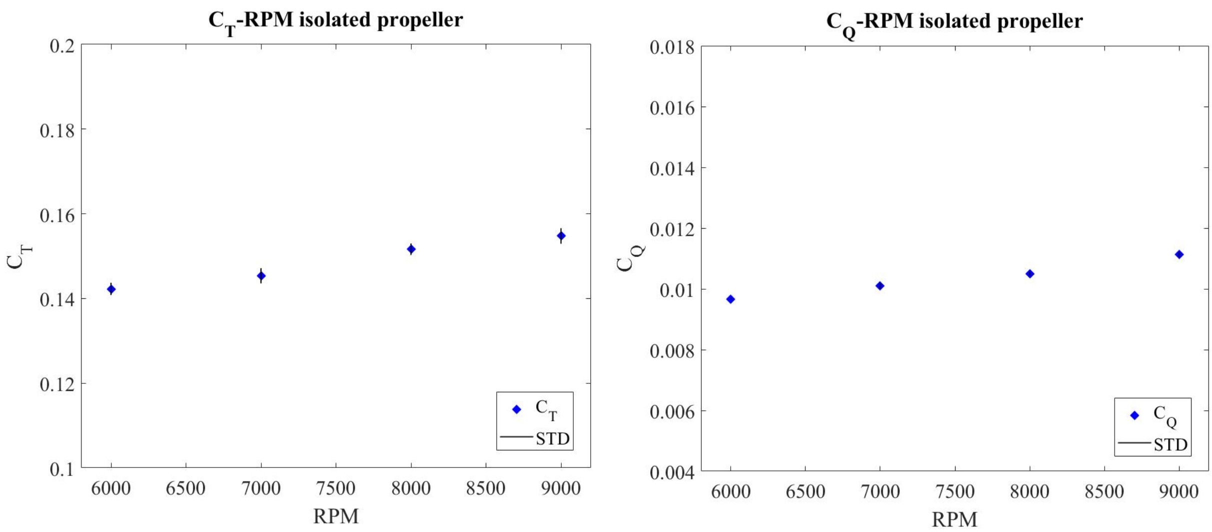


Figure 3.1: Thrust and torque coefficients of the single propeller case.

## Isolated Propeller Performance

Figure 3.1 shows the behaviour of the thrust and torque coefficients varying the RPM for the four rotational velocity tested, and their respective interval of confidence at 95% (this interval is obtained triplicating punctually the standard deviation of the measurements acquired).

The single propeller configuration was tested once during the experimental campaign, in particular at its the very beginning.

The propeller tested is the one that will be labelled as the reference one, since it will be taken as reference for the following analysis.

As it is expected both the thrust and the torque coefficients increase with the RPM, this means that increasing the velocity of rotation the aerodynamic loads on the blades are higher. In particular, it is possible to see that the aerodynamic loads behave almost linearly varying the RPM.

## Side-by-side Propellers Performances

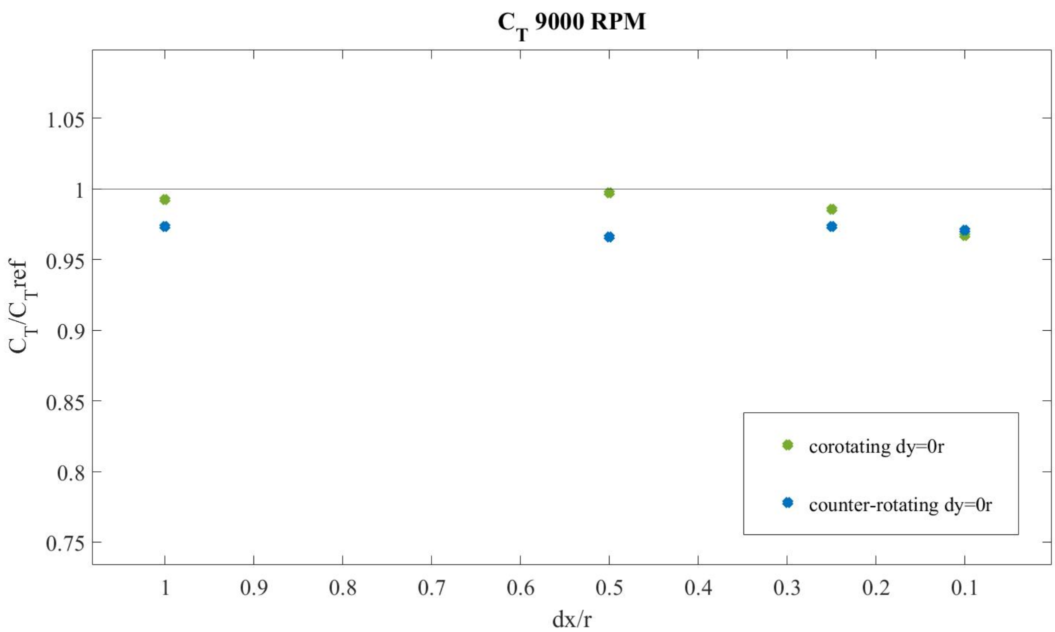


Figure 3.2: Thrust coefficient of the co-rotating and counter-rotating tandem propellers case with $dy = 0r$.

The following results concern the tandem propellers configuration. The tandem configuration was tested varying the tip-to-tip distance between the propellers and also the disk-to-disk distance. To vary the value of $dy/r$ the reference propeller was kept fixed while the second propeller was moved forward to create a kind of disturb so that its wake could interact with the reference one. Accordingly, to this observation the coefficients shown refer all to the aforementioned reference propeller, that is the one that became of interest to be analysed. The second propeller is supposed to keep its performances almost stable varying its position since it feels in a much lighter way the influence of the other one. Figure 3.2 shows the thrust coefficients of the reference propeller for all the analysed side-by-side cases with RPM 9000, the results are normalised with respect to the isolated propeller configuration coefficients of RPM 9000. The data selected for the normalization are the one obtained the first day of the campaign. In case of co-rotation the propellers' blades rotate clockwise. Indeed, in case of counter-rotation the blades of the second propeller were changed and replaced with right handed blades, in this way the direction and sign of the thrust are always the same and the wake is always propagating in the same direction.

Concerning the $C_T$, its adimensionalised values are always lower than 1, this mean that the reference propeller in the tandem propellers configurations always works less efficiently than in the isolated case. In the case with $dy = 0r$, as it is expected, the trend of the coefficients is to decrease with the relative tip-to-tip distance $dx/r$, where $r$ is the ray of the blade. Getting closer the two propellers influence more heavily each other reducing their performances, in particular the performances of the reference propeller are reduced. Moreover, it is possible to observe how the co-rotating case shows better performances with an improvement up to $2,5\%$, its $C_T$ values are also closer to 1 meaning that they are more similar to the undisturbed isolated propeller case.

The trend to reduce the $C_T$ with the tip-to-tip distance is the one expected from literature since was already observed experimentally by many other researchers for example Wenwu Zhou [14] and Austin David Thai [10] and numerically by Alvarez [4].

## Staggered Tandem Propellers Performances

Also, the tandem staggered configurations were tested, the ones with $dy = 0,5r$ were tested both co and counter-rotating while the ones with $dy = 1r$ were tested just with co-rotating blades. The performances obtained are still referred to the reference propeller and normalised with respect to the isolated case. Varying the relative tip-to-tip distances between the two propellers the difference in the thrust coefficient is not that relevant, but still the tendency is to reduce the thrust with the two propellers getting closer. In this case it is more difficult to understand which verse of rotation is optimal for the performances.

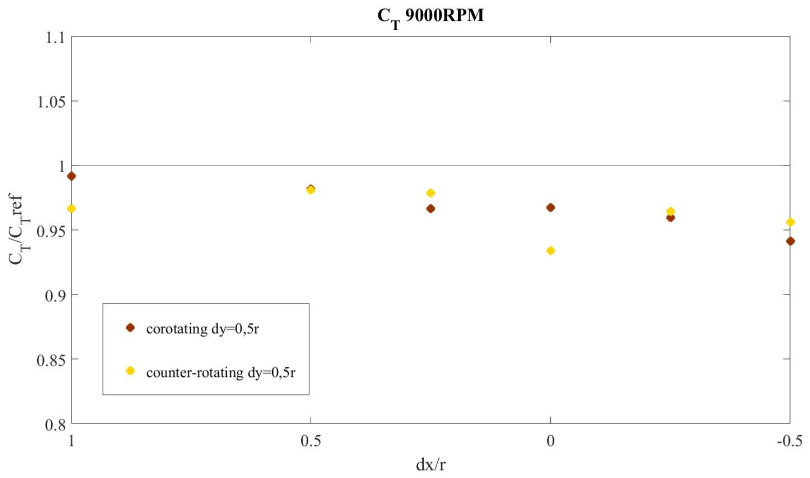


Figure 3.3: Thrust coefficient of the co-rotating and counter-rotating tandem propellers case.

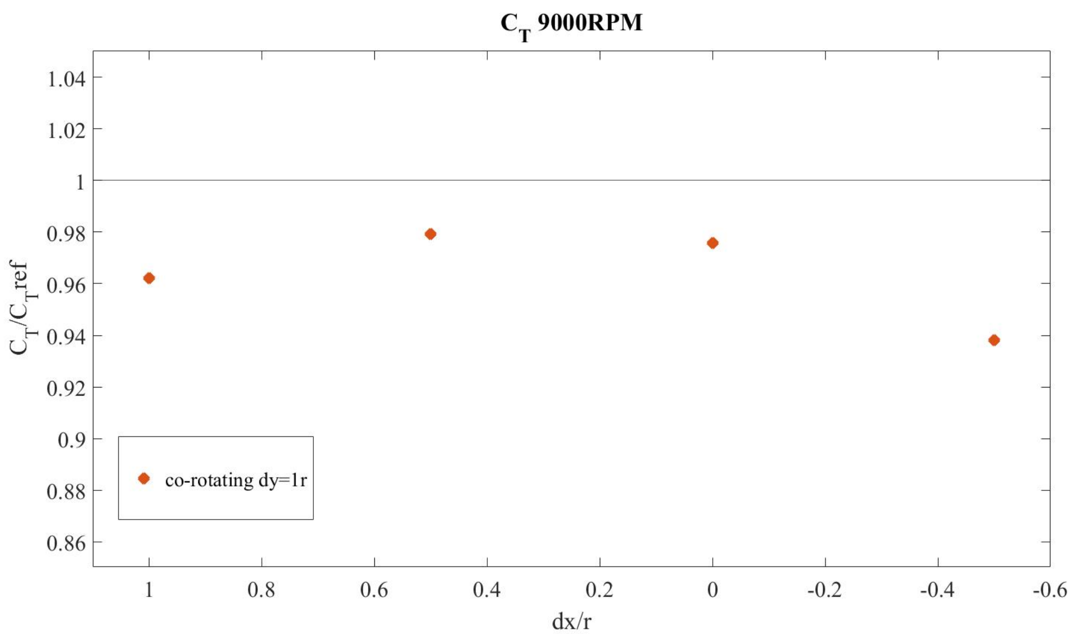


Figure 3.4: Thrust coefficient of the co-rotating and counter-rotating tandem propellers case.

Moreover, fixed the parameter $dx/r$ and varying the $dy/r$ value for both co-rotating and counter-rotating configuration the difference in the performances is felt less. This means that the disturbance of the second propeller should be reduced working on the tip-to-tip distance and not on the forward displacement. Let's consider the case of $dy = 0,5r$ and $dy = 1r$, figure 3.3 and figure 3.4; once more the coefficients fall when the propellers get close enough, in particular, when there is overlapping between the reference propeller and the moved back propeller. This effect is still due to the fact that the reference propeller gets into the wake of the advanced one, and the vortexes produced interact with the blades of the reference propeller creating a loss of thrust. When the blades are not caught into the wake, they push still air creating a $u_\infty$ that is just the self-induced one and the pitch angle is close to the ideal one. Instead, when the blades are caught into the wake there is an additional velocity that sums to $u_\infty$, it locally varies the velocity vectors composition and changes the pitch angle that, being reduced, creates consequently a loss of thrust.

### 3.0.2. Thrust Fluctuations

An interesting behaviour could be observed analysing the thrust fluctuations. As a matter of fact, while the data reported in the previous plots are just averaged values on time of the thrust and the torque coefficient, it should be pointed out that these values actually oscillate in time around an average. The amplitudes of fluctuation of the thrust coefficient are reported in figure 3.5a, 3.5b and 3.5c adimensionalised with respect to the fluctuations of the thrust of the isolated propeller. It is possible to see that while the two propellers are far enough the fluctuations of the reference propeller correspond to the isolated propeller ones, while the amplitude increases decreasing their relative distance. Indeed, while the thrust coefficient varies slightly changing the relative distance (the variation is 7% at its maximum), the thrust fluctuations variations with respect to the isolated propeller case are much higher since they get to be $3,7$ times the isolated propeller fluctuations in the worst case scenario. This effect is due to the intensified rotor-to-rotor interactions. To show this behaviour the cases of $6000 RPM$ has been chosen, this is the case with the lowest RPM. Indeed, the higher RPM results do not show a regular behaviour, this is probably due to the fact that more mechanical vibrations are induced on the structure holding the propellers increasing the RPM. This same behaviour was observed and analysed by Wenwu Zhou and its crew [14].

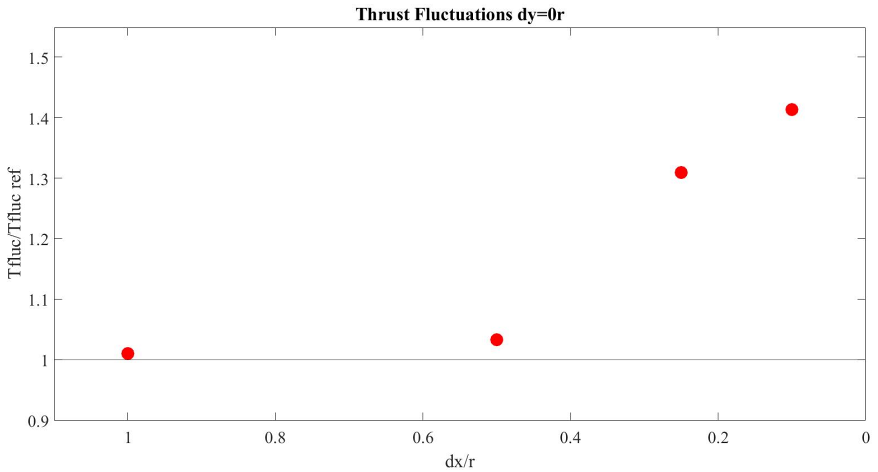


(a) Normalised thrust fluctuations for the tandem propeller case with $dy = 0r$ varying the distance.

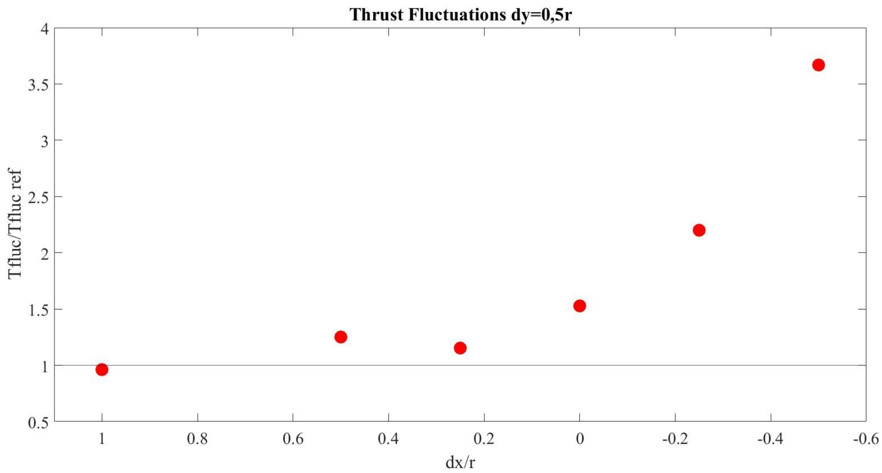


(b) Normalised thrust fluctuations for the tandem propeller case with $dy = 0,5r$ varying the distance.

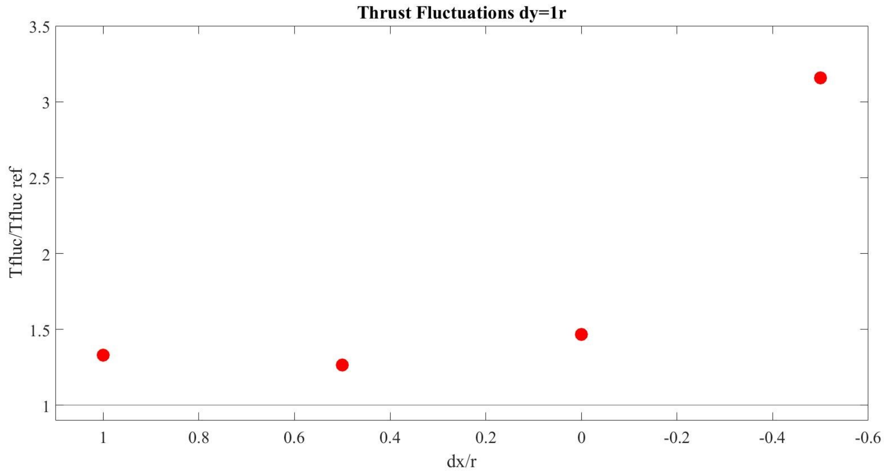


(c) Normalised thrust fluctuations for the tandem propeller case with $dy = 1r$ varying the distance.

Figure 3.5: Normalised thrust fluctuations.

### 3.0.3. Propeller acoustic

Different post-processing tools are adopted to analyse the acoustics of the two propellers: the analysis of the spectra was performed throughout PSD (power spectral density), the broadband interpolation, the OASPL analysis and the A-weighted OASPL analysis.

## Signal processing

As a first step to post-process, all the signals acquired were filtered using a band-pass filter, the representation of the filter can be seen from figure 3.6. Considering that the cut-off frequency of the chamber is $f_{CUT} = 150Hz$ and the sampling frequency is $f_S = 25600Hz$ the filter is designed in this way:

- $Fstop1 = 100Hz$ First Stop-band Frequency;
- $Fpass1 = 150Hz$ First Pass-band Frequency;
- $Fpass2 = 10000Hz$ Second Pass-band Frequency;
- $Fstop2 = 12800Hz$ Second Stop-band Frequency.

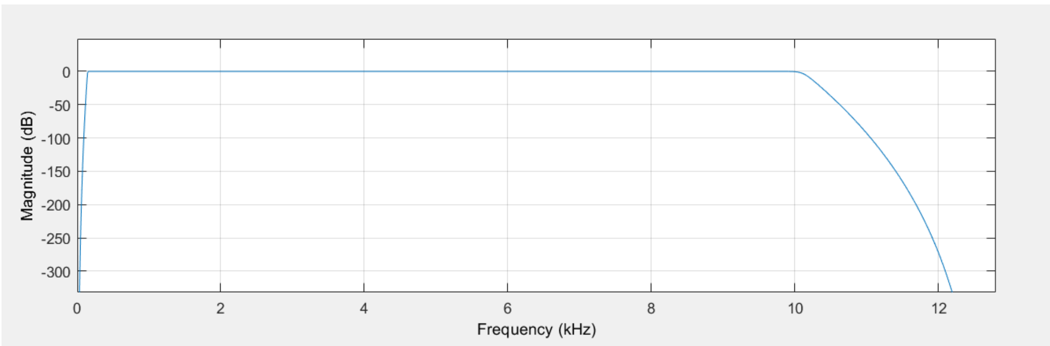


Figure 3.6: Passband filter adopted.

This tool is useful since it allows to filter the wider acoustic fluctuations that are perceived by the microphones in the wake of the propeller. These fluctuations are read by the microphones but they are due to the presence of the eddies in the wake and do not have any acoustic meaning. In the following figure 3.8 is represented the signal captured by the seventh microphone (from the front) positioned at $\beta = 180°$, exactly in the wake of the propeller, in the single propeller configuration at $9000RPM$. The signal, before being processed, presents wide fluctuations in time (this means low frequency fluctuations), that are filtered by the band-pass filter damping the lower frequencies.
At the beginning of the campaign the empty anechoic chamber was acoustically tested

three times throughout the microphones and the OASPL plot was obtained, this plot is reported in figure 3.7.

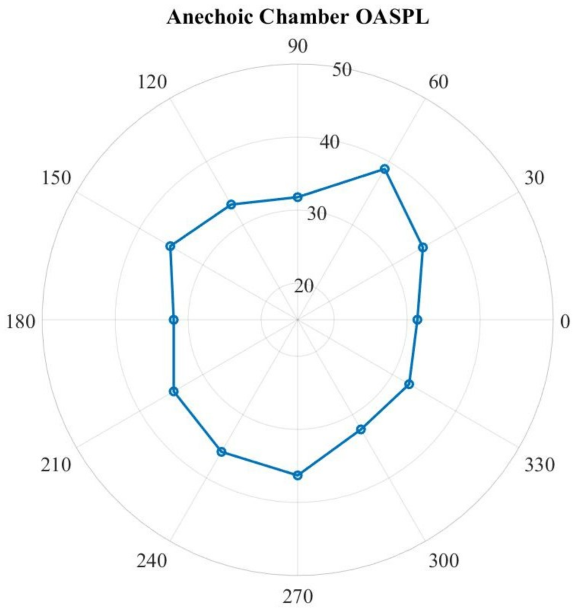


Figure 3.7: OASPL of the empty anechoic chamber acquired at the beginning of the campaign.

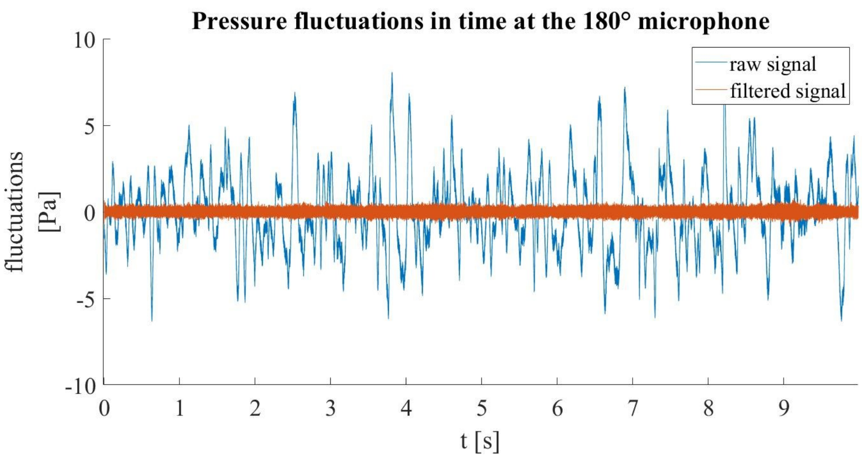


Figure 3.8: $\beta = 180°$ microphone filtered and not filter pressure fluctuations.

### 3.0.4. Power Spectral Density

After being processed, the signal is used to obtain the power spectral density. Since the fluctuations in time are in $Pa$ then the PSD (that is an energy) results to be in $Pa^2/Hz$, but, to better understand the values of the peaks in the spectra, the PSD is converted to $dB$ throughout the sound pressure level, $SPL$, formula(3.1) function with a pressure reference of value $P_{REF} = 20 * 10^{-6}$.

$$SPL = 20log_{10}(P/(P_{REF})) \tag{3.1}$$

## Isolated Propeller Power Spectral Density

Figure 3.9 shows the acoustic spectra acquired at the microphone positioned at $\beta = 0°$ (in the front of the propeller) varying the RPM for the case of the isolated propeller, additionally also the spectra of the motor are reported. The noise of the motor was obtained from same experimental set up removing the hub and the blades from the propeller.

The engine PSD is not reported for the case of $6000RPM$, this is due to the fact that the hub starts rotating after giving a minimum amount of power to the engine, this minimum level increases in case of just the presence of the engine because the system, without the hub and the blades encounters less resistance and, therefore, with the same power level the system rotates at higher RPM.

The tonal peaks in the PSD are caused by sources that repeat themselves exactly during each rotation, they are well defined and surrounded by broadband noise, non-periodic signal generated from the turbulence impacting on the blades [6] (page 401). The main peak appears at the blade passing frequency (BPF)[1], this means that the major contributor to the oscillations of the pressure is coming from the passage of the blade. A fixed observer sees, since the propeller is a 3-blade, the blade passage three times per rotation generating the same oscillations each time, which is the reason why the frequency of the peak is three times the frequency of rotation. For the same reason it is possible to spot other lower peaks at frequencies multiple of the BPF, 2th-8th BPFs harmonics, these are still due to the passages of the blades but produce noise at higher tones (different harmonic). It is possible to also identify another tonal peak at lower frequency in particular, for each RPM analysed, at the frequency of rotation, this peak becomes much more marked increasing the RPM and its easily identifiable at $9000RPM$. This peak, as the plot justifies, could be due to the presence of the motor which has its own tonal frequencies.

[1]The blade passing frequency is the frequency at which a foxed external observer sees the pressure perturbation coming to him. This corresponds to the frequency at which he sees the passage of the blade. For a $N$ blade propeller corresponds to $N$ times the frequency of rotation.

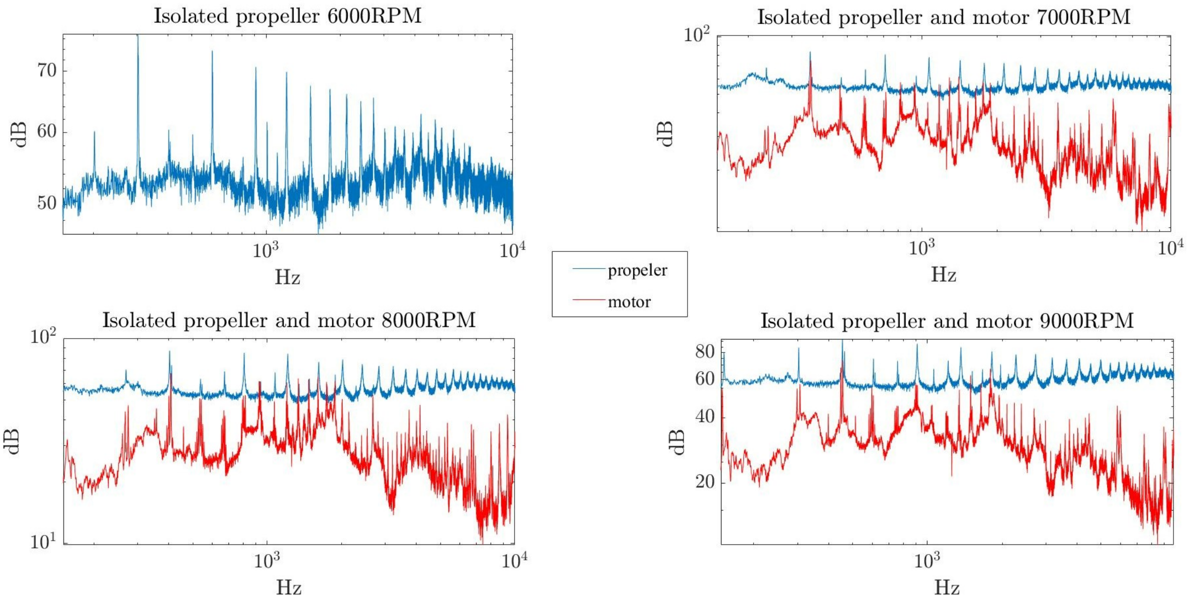


Figure 3.9: PSD of the single propeller configuration varying the RPM with the addition of the PSD of the motor.

The tonal noise can be analysed to identify its main contributor, since the air is still in the considered test case, this depends just on the rotor tip Mach. From the Ffowcs-Williams and Hawkings equation [6] (page99) it is possible to understand that the tonal noise is produced by various sources:

- Monopoles, thickness noise, that becomes important just at high Mach tip ($Ma = 0,7$), this represents the contribution from the blade surface motion. Considering that the Mach tip reached in the different test increasing the RPM is around $Ma = 0,4$, then this contribution is not relevant for the case of study.
- The second type of noise is the loading noise that is produced by the dipole term in FWH. This happens because a fixed observer sees the forces on the blade varying their direction during the revolution (while in the blade-base reference system they do not), this behaviour results in the generation of a sound wave.
- Concerning the engine, the broadband noise is much reduced since there is no flow produced since there are no blades. The PSD is characterised also by some defined peaks, this is tonal noise and can be due to the fact that the engine is an electrical one and works throughout the rotation of a series of magnetic poles.

## Side-by-side Propellers Power Spectral Density

In the following part the case of side-by-side $dy = 0r$ propellers is analysed for $9000 RPM$. Figure 3.10 shows the PSD of this configuration varying the relative tip-to-tip distance between the two propellers.

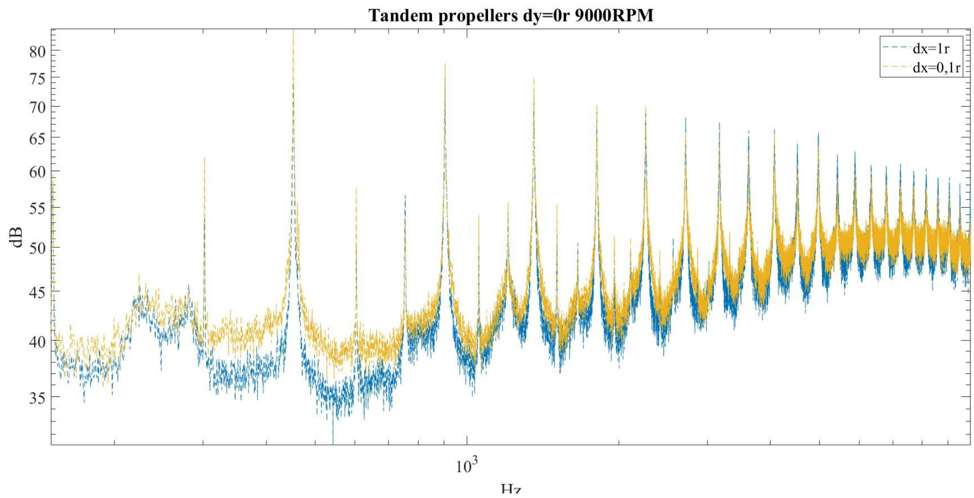


Figure 3.10: PSD of the tandem propellers configuration with $dy = 0r$ varying the relative distance.

While the two propellers are positioned far away, $dx = 1r$, their interaction is limited and the noise produced is lower than the other case, in fact the PSD, for both tonal and broadband noise is the lowest. Reducing the tip-to-tip distance the two propellers feel more heavily their mutual presence and the PSD increases both in tonal and broadband components resulting in an higher noise production, the closest distance, $0, 1r$, in which the tips of the blades are almost touching, is the one with the highest PSD, in particular is possible to see a visible gap in the broadband noise between it and the case of $dx = 1r$. The increment in the PSD happens both in the tonal and the broadband components. Since for low Mach number flows the main contributor to tonal noise is the loading noise, it is possible to associate the increase of the peaks in the PSD decreasing the distance with the increasing of the thrust fluctuations mentioned before. Also, broadband noise shows a significant increment decreasing the relative distance, and since the main contributor to broadband noise are the vortexes, then the wake is supposed to increase its turbulence decreasing the distance between the two propellers.

This behaviour was already discovered by Wenwu Zhou [14] and his team, the same concept that they stated is also valid here, the broadband noise increases with the presence of turbulent flow structures and shear layers in particular: secondary flow distortions, blade trailing edge vortexes, and tip vortexes. Also the turbulent kinetic energy and the forces fluctuations play an important role as it is highlighted from T. Carolus [5], since their level also determine the intensity of the broadband noise. As a matter of fact, the propellers show increasing TKE level and force fluctuations as the separation distance decreases.

In figure 3.11 is also reported the engine PSD in the case of side-by-side propeller configuration that can be compared to the case of $dx = 0,1r$ and $9000RPM$. Similarly, as it was for the isolated motor, the presence of the motor is relevant since its spectrum is characterised by both tonal peaks and broadband component. The broadband level is much less intense than the respective test done on the actual propeller since the main contributor to the broadband noise is the stochastic interaction of turbulent structure of the wake with the body. Tonal peaks are still present and depend on the mechanical characteristics of the motor, in particular the PSD of the motor presents a peak around the 1st BPF that generated a relevant peak in the spectrum of the propeller.

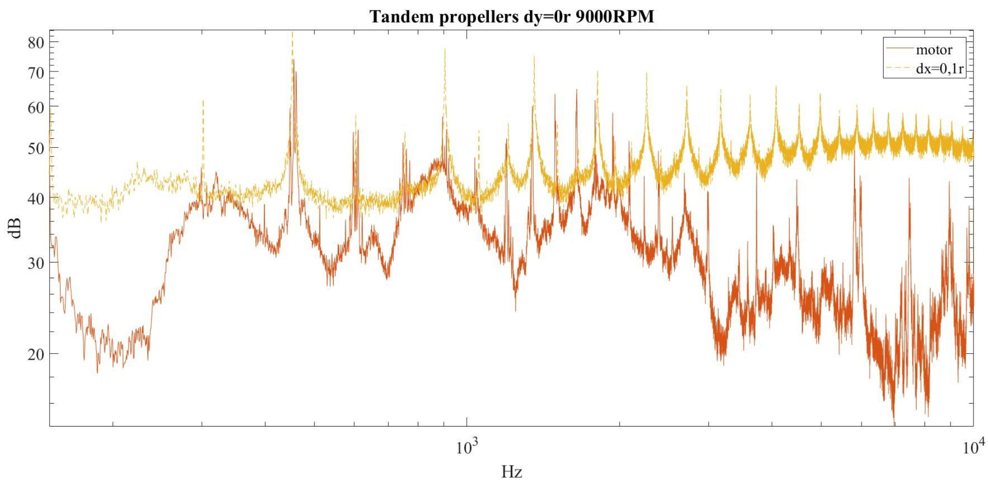


Figure 3.11: PSD of the tandem prop configuration with $dy = 0r$ at distance $dx = 0,1r$, with the addiction of the tandem prop engine PSD.

## Staggered Tandem Propellers Power Spectral Density

In the following section the case of the tandem propeller configuration with $dy = 0,5r$ is analysed, differently from the previous configuration here is possible to realise the overlapping of the propellers' blades with the advanced propeller that produces a wake that impacts on the blades of the other one. In figure 3.12, are reported the PSD, acquired from the microphone positioned at $\beta = 0°$, for relative tip-to-tip distance of $0,25r$ and $-0,25r$ with $dy = 0,5r$. At distance smaller than $0r$ the back propeller starts to interact heavily with the wake of the advanced one and the noise generated increases, since the PSD curves are higher both in broadband and tonal noise. There is a visible gap between the PSD of the broadband noise in case of impact of the wake on the blades and nacelle and distance bigger than 0, marking a substantial difference in the noise produced by these configurations. These two increments are still due to the increasing thrust fluctuations and increasing turbulence in the wake interacting with a solid body as it was explained before.

In particular it is possible to understand where the increasing thrust fluctuations are coming from: a change in angle of attack can be produced when the tip vortexes are ingested into the second rotor and when the blades pass near the core of the vortex, this causes a sudden change in the blade load and therefore an increase in the fluctuations.

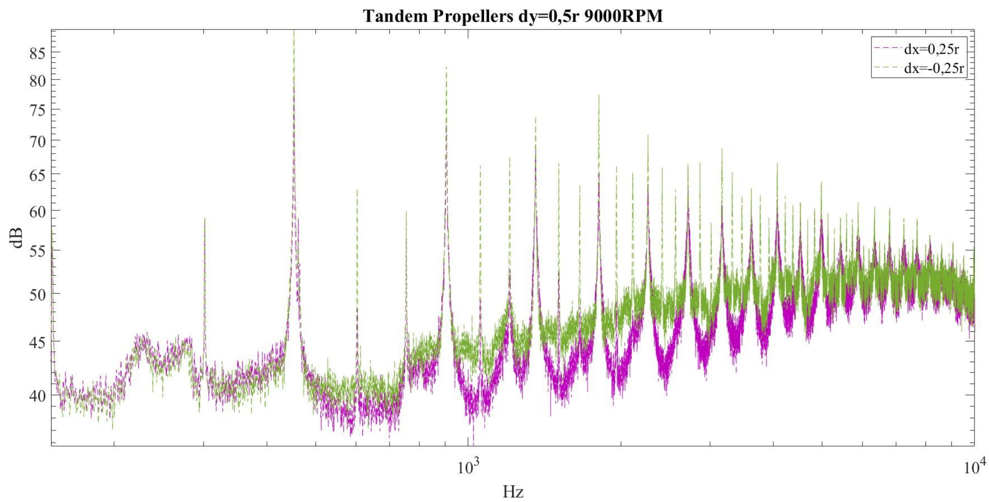


Figure 3.12: PSD of the tandem prop configuration with $dy = 0,5r$ at various distances.

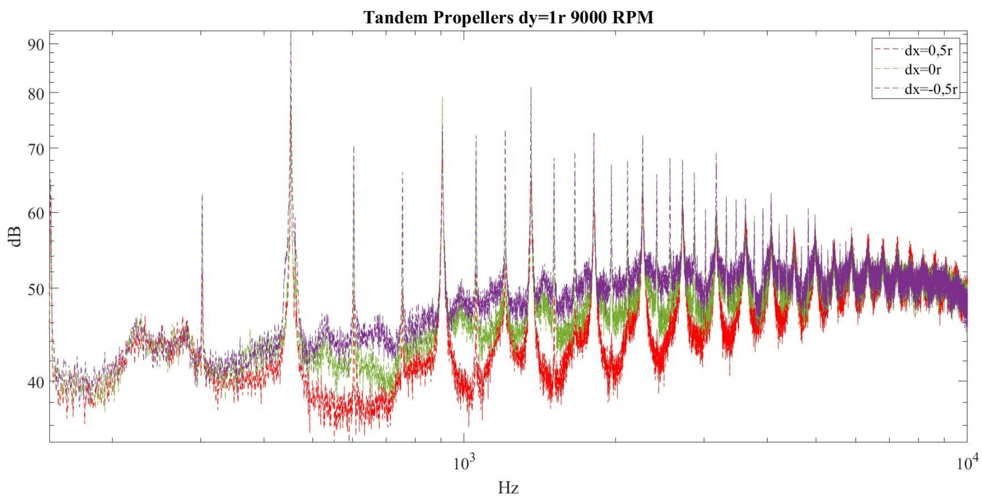


Figure 3.13: PSD of the tandem prop configuration with $dy = 1r$ at various distances.

This interaction produces a particular thumping noise and it is the one that mainly bothers human hearing in helicopter noise. This kind of noise could be eliminated if the wake is ingested differently but the operational conditions could not always be so easy to change without consequences [6] (page 402). A similar behaviour occurs also with the case of $dy = 1r$ and is reported in figure 3.13 also here is easy to spot the gap between the different relative distances in the broadband noise component indicating an increase in the vortex production for the close distances. The behaviour is similar to the previous case since the back propeller is still hit by the wake when overlapping of the blades happens.

### 3.0.5. Overall Averaged Sound Pressure Level Analysis

The overall averaged sound pressure level (OASPL) is a method to quantify the noise considering both tonal and broadband components, and it is measured in decibels (dB). It consists in the integral over the frequencies of interest of the spectrum of a sound signal. In particular it is defined here as the integral of the acoustic spectrum between the frequencies of $f = 150Hz$ (cut-off anechoic chamber value) and $f_S/2$ (frequency until which the spectrum is still dependable). For every microphone placed in the chamber there is one resultant value of OASPL averaged over the time and therefore the following plots, will be polar plots reporting every 30° the value of the corresponding OASPL.

#### Isolated Propeller Overall Averaged Sound Pressure Level

The first case that will be examined is the case of isolated propeller configuration, figure 3.14. The OASPL is shown for all the different RPM values measured, in the cases of 7000, 8000 and $9000RPM$, are also reported the values of the isolated engine OASPL. Concerning the case of $6000RPM$ the engine noise is not shown for the aforementioned reasons. Since the configuration is symmetric around the nacelle axis also the OASPL results to be symmetric around the same axis. Moreover it is possible to notice another behaviour, the OASPL value is at its maximum at the front of the propeller ($\beta = 0°$ and $\beta = 180°$), where, as expected from theory the directivity of the noise should be the greatest, indeed the OASPL decreases almost monotonously towards the sides. The greatest directivity its towards $\beta = 0°$ since the main contributor to noise is the loading component whose main direction of propagation is the vertical one. This same behaviour is analysed also by Wenwu Zhou [14]. Indeed, the thickness noise propagates mostly on the plane of rotation of the blades, but this component is much less intense here.

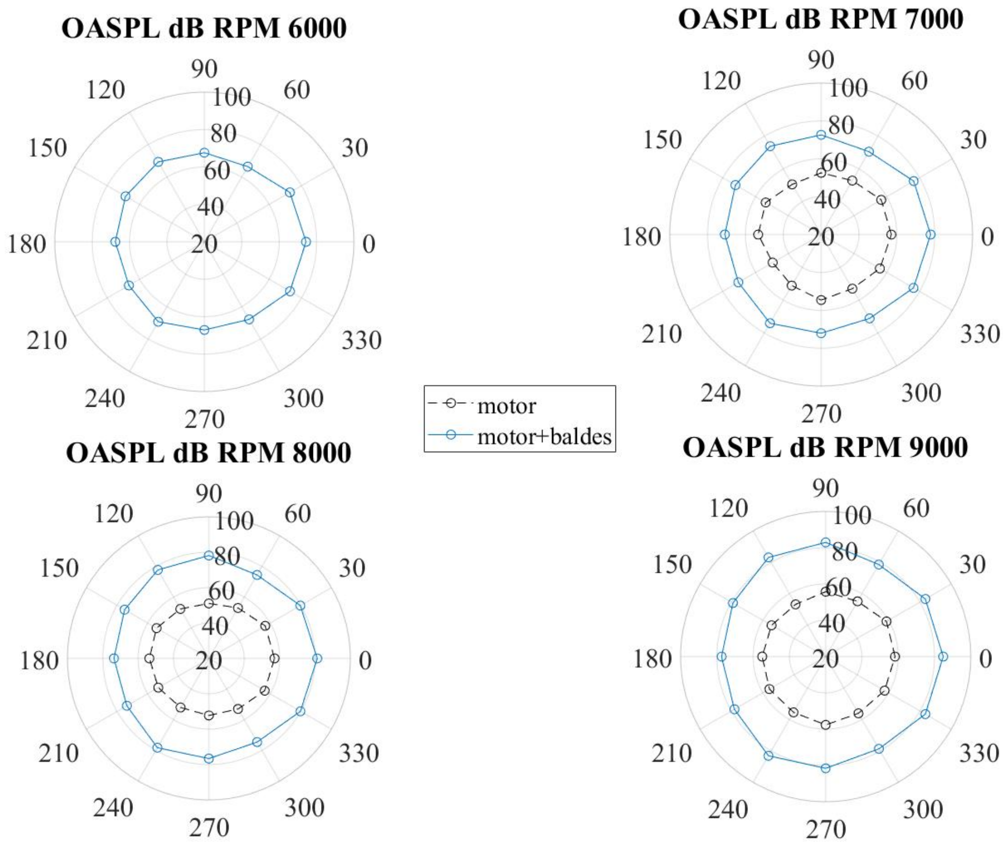


Figure 3.14: OASPL of the single propeller configuration with also reported the engine noise.

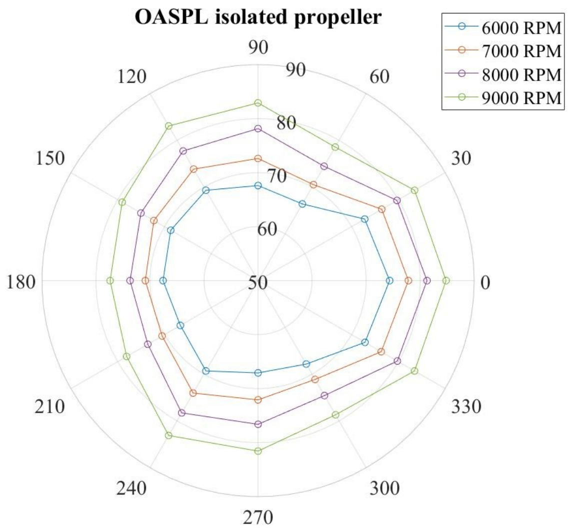


Figure 3.15: OASPL of the single propeller configuration varying the RPM.

Figure 3.15 shows the OASPL for the single case propeller varying the RPM value. Averaging the values of the OASPL over the angles at different RPM it is possible to see that increasing the RPM of 1000 the decibel acquired increases almost of $3,5dB$.

### Side-by-side Propellers Overall Averaged Sound Pressure Level.

Figure 3.16 shows the OASPL in case of $dy = 0r$ at $9000RPM$ varying the relative distance between the two propellers. It shows also the respective OASPL of the two motors. Differently from the analysis of the PSD, figure 3.10, that shows a more accurate noise content of the signal over the frequencies, the overall averaged SPL does not show a remarkable difference in the values obtained for each angle since the curves for the different distance are almost overlapping. The only curve that is discernible form the other is the one of $dx = 1r$ relative distance that show a slight decrease in the OASPL, meaning that for this distance the two propellers feel less the presence of the other respectively. Indeed, for the closer distances, they feel a slight interaction, this interaction remains limited since, in the case of $dy = 0r$, the propellers do not interact with the wake. The behaviour of the OASPL is still symmetric around the nacelle axis because, also with the introduction of the second propeller the configuration is still symmetric.

### Staggered Tandem Propellers Overall Averaged Sound Pressure Level.

Figure 3.17 shows the behaviour of the OASPL over the angles varying the relative distance between the propellers in case of $dy = 0,5r$ at $9000RPM$. While the two propellers are not overlapping the interaction with the wake of the back one is limited or absent and for this reason the obtained OASPL curve ($dx = 1r$) is the lowest. At relative distance $dx = 0r$ the wake of the advanced propeller starts to impact on the tip of the blades of the other one globally increasing the noise the averaged increase of decibel with respect to the other not overlapping cases is of $2,4B$. For the other cases of higher overlapping the noise intensity increases more. In the case of relative distance of $-0,25r$ the averaged increase in the decibel is $2,4dB$, while for the distance of $-0,5r$ the increase with respect to the previous distance is $1,3dB$. A significant increase of noise level at these distances is due to the fact that the wake of the advanced propeller impact on the blades of the other one producing a "thump" noise. The plot of the OASPL remains still almost symmetric with respect to the middle plain of the chamber even if the configuration is not completely symmetric, the symmetry is broken by advancing the second propeller. This happens probably because the source of noise is felt as pointwise by the microphones because they are placed far enough.

To sum up some of the statements said before the OASPL is a function of both the relative distance between the two propeller ($d/r$) and the azimuthal angle, in particular the OASPL increases decreasing the distance of the two propellers and increases from the side towards the front of the propeller assuming the shape of a three-lobe.

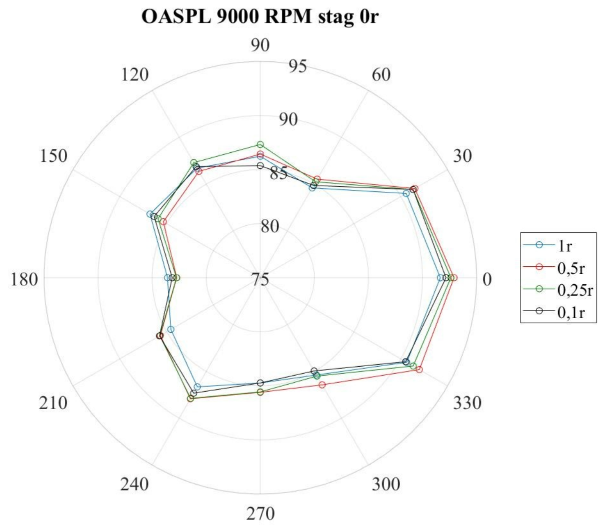


Figure 3.16: OASPL of the tandem propeller configuration with $dy = 0r$ varying the relative distance at $9000RPM$.

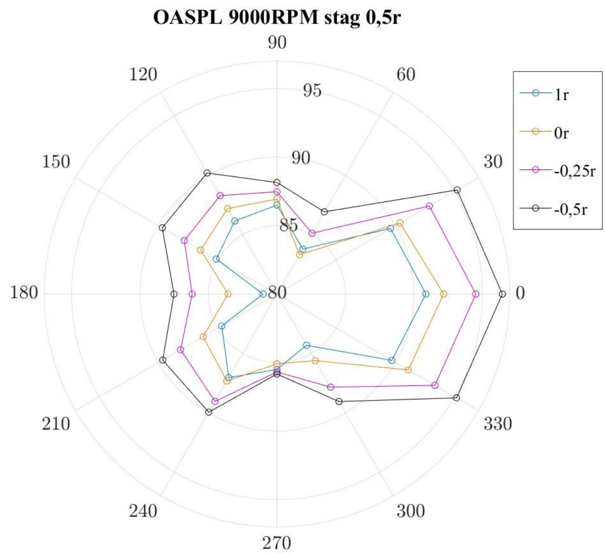


Figure 3.17: OASPL of the tandem propeller configuration with $dy = 0,5r$ varying the relative distance at $9000RPM$.

Figure 3.18 shows the behaviour of the OASPL over the angles varying the relative distance between the propellers in case of $dy = 1r$ at $9000RPM$. Even if the relative distances tested are less than the previous case, is still possible to identify the same behaviour. The decibels remain almost constant over the angles until there is an overlapping of the propeller and the wake produced by the advanced propeller interact with the other one producing more noise.

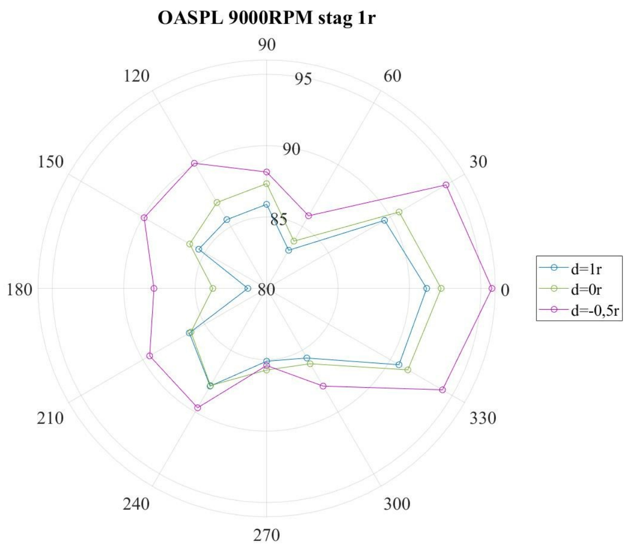


Figure 3.18: OASPL of the counter-rotating tandem propeller configuration with $dy = 0r$ varying the relative distance at $9000RPM$.

## Comparison Between Different Stags

Figure 3.19 shows the comparison between different cases of stag OASPL. The value of the stag seems not to influence much the production of noise since it is not possible to identify a trend with a variation of the value $dy/r$.

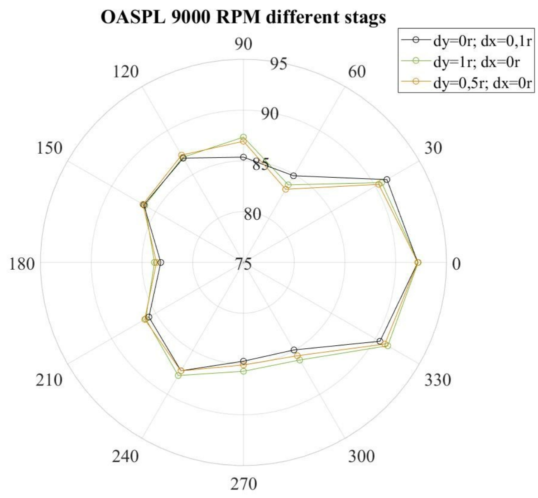


Figure 3.19: Comparison of the OASPL between different stags.

### 3.0.6. Comparison between counter and co-rotating configurations

Figures 3.20a, 3.20b and 3.20c show the comparison between OASPL of co-rotating and counter-rotating configurations with $dy = 0r$, $9000rpm$ at various distances. The behaviour of the noise intensity is unexpected since the counter-rotating configuration is the best (lowest noise) at different angles for bigger distances, while, with the two propellers getting closer, there is an inversion and the best one becomes the co-rotating configuration. This result is in accordance to the literature since, for close distances also Austin David Thay [10] achieved the same result stating that the counter-rotating case, for distance up to $0,28d/r$, is more or less $1dB$ louder. To better understand this behaviour an analysis of the PSD of the two extreme cases has been done. Figure 3.21a and 3.21b report the PSDs for $dy = 0r$ registered at the $\beta = 0°$ microphone:

- The PSD for $dx = 1r$, figure3.21a shows that the co-rotating case is the worst one since both broadband components and tonal peaks are slightly higher than the counter-rotating case. Instead at lower frequency the broadband component for the counter-rotating case is the highest, but, knowing that the OASPL is an integral over all the frequencies, this contribute is cancelled by the one coming from higher frequencies.
- The PSD for $dx = 0,1r$, figure3.21b shows that the counter-rotating case is slightly more noisy since both broadband components and tonal peaks are slightly higher

than the co-rotating case.

A trend like the one observed before is also visible for the staggered case. Figures 3.22a, 3.22b, 3.22c and 3.22d show the comparison between counter and co-rotating case for $dy = 0,5r$ at various distances. Once more at higher distances between the two propellers the co-rotating case shows globally the worst acoustic performance, while getting closer, in particular with the overlapping of the two propellers there is an inversion and the counter-rotating case becomes the worst one.

The PSDs reported in figure 3.23 are the ones for the case of $dy = 0,5r$ and $dx = 0r$ at the $\beta = 0°$ microphone since there is a remarkable gap between the co-rotating and counter-rotating values of the OASPL. Here is possible to see that the broadband component for the co-rotating case is visibly higher and also the tonal peaks, for the same case are slightly more pronounced.

This behaviour could be explained thinking about the physics of the wake produced. The increment in the broadband component for close distance could be due to the fact that, since the vortexes produced by the advanced propeller are co-rotating with the ones produced by the other propellers, their momenta sum up increasing the TKE. For the counter-rotating case, instead the TKE is partially lost since the particles are rotating in opposite directions. Instead, when there is overlapping of the blades the counter-rotating vortexes could affect more the oscillations of the thrust forces bringing to higher oscillation of angle of attack, as a result the tonal peaks are higher.

To better understand this behaviour a study on the standard deviation has been added and reported in figure 3.24 for the case of $dy = 0r$. In the plot is represented, with the mean values of the SPL, also their interval of confidence at 95% (3 times the standard deviation). The mean value of the SPLs shows the behaviour described before, but their confidence intervals intersect meaning that, there is a certain probability that the two plots could invert their trend at least for certain angles. In any case the average values trend tends to be the one analysed before, but it should be kept in mind that the counter-rotation can lead to a decrease in the performances therefore the best case results to be the co-rotating one.

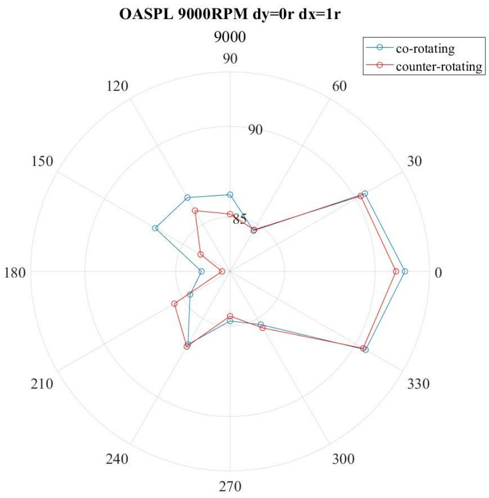


(a) OASPL $dy = 0r$ and $dx = 1r$ comparison between counter and co-rotating configurations.

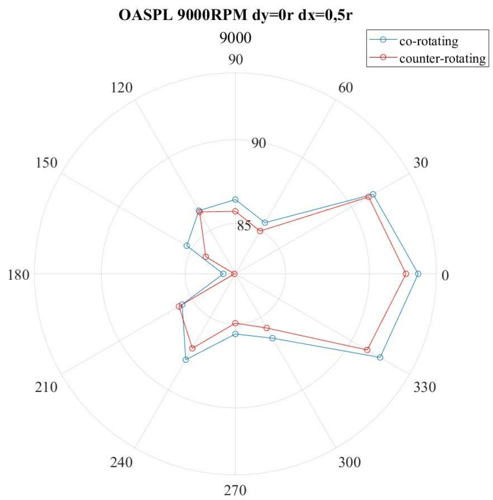


(b) OASPL $dy = 0r$ and $dx = 0,5r$ comparison between counter and co-rotating configurations.

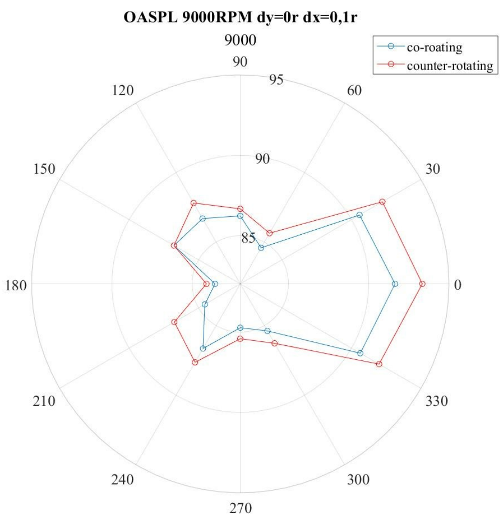


(c) OASPL $dy = 0r$ and $dx = 0,1r$ comparison between counter and co-rotating configurations.

Figure 3.20: OASPL $dy = 0r$ comparison between counter and co-rotating configurations.

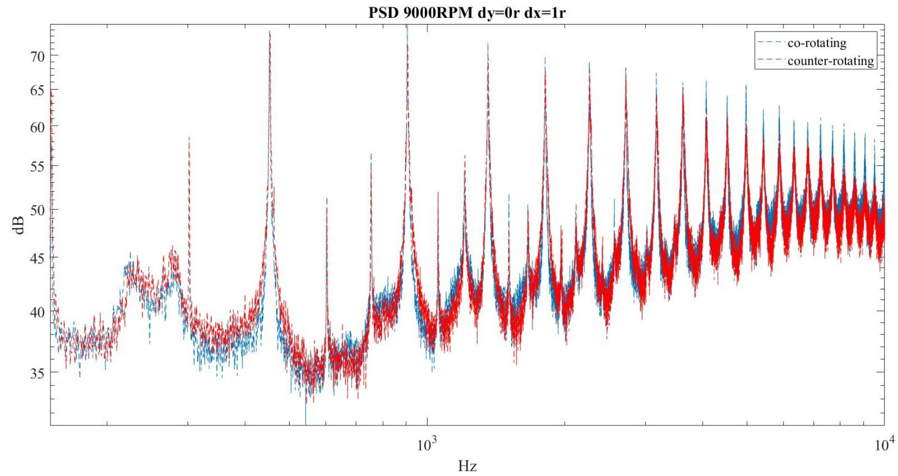


(a) PSD $dy = 0r$ and $dx = 1r$ comparison between counter and co-rotating configurations.

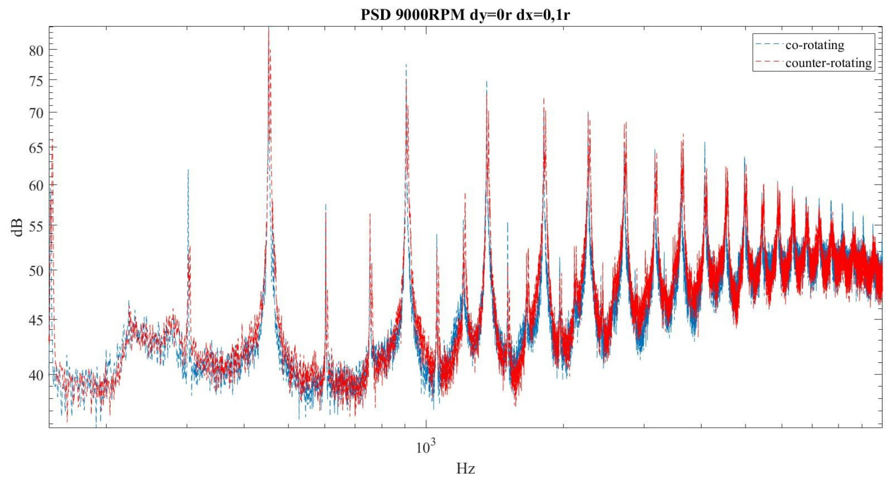


(b) PSD $dy = 0r$ and $dx = 0,1r$ comparison between counter and co-rotating configurations.

Figure 3.21: PSD $dy = 0r$ comparison between counter and co-rotating configurations.

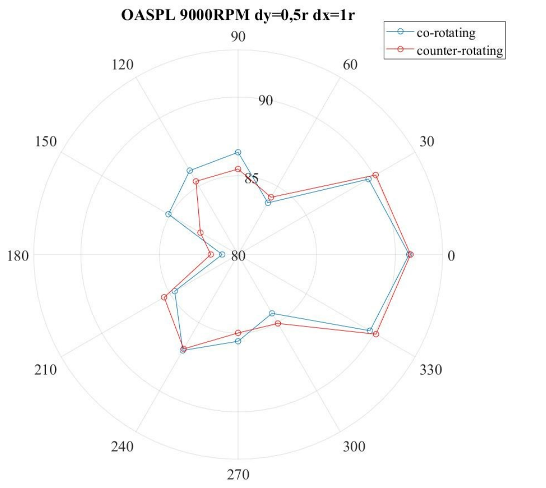


(a) OASPL $dy = 0,5r$ and $dx = 1r$ comparison between counter and co-rotating configurations.

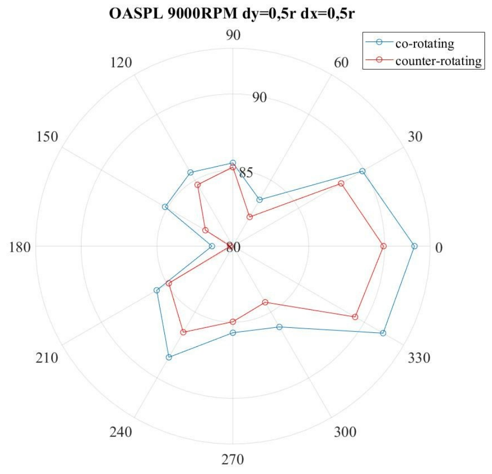


(b) OASPL $dy = 0,5r$ and $dx = 0,5r$ comparison between counter and co-rotating configurations.

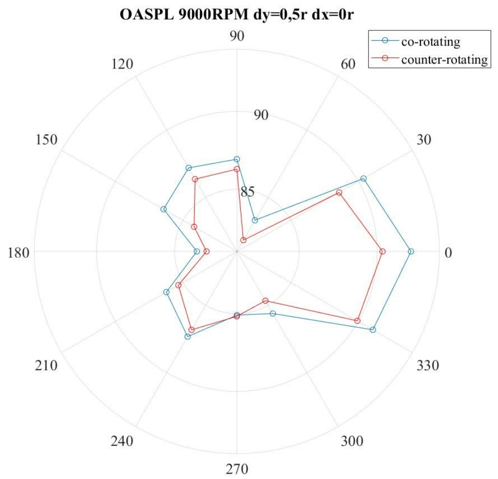


(c) OASPL $dy = 0,5r$ and $dx = 0r$ comparison between counter and co-rotating configurations.

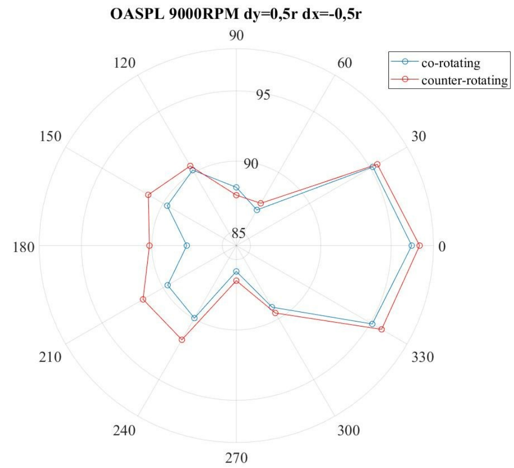


(d) OASPL $dy = 0,5r$ and $dx = -0,5r$ comparison between counter and co-rotating configurations.

Figure 3.22: OASPL $dy = 0,5r$ comparison between counter and co-rotating configurations.

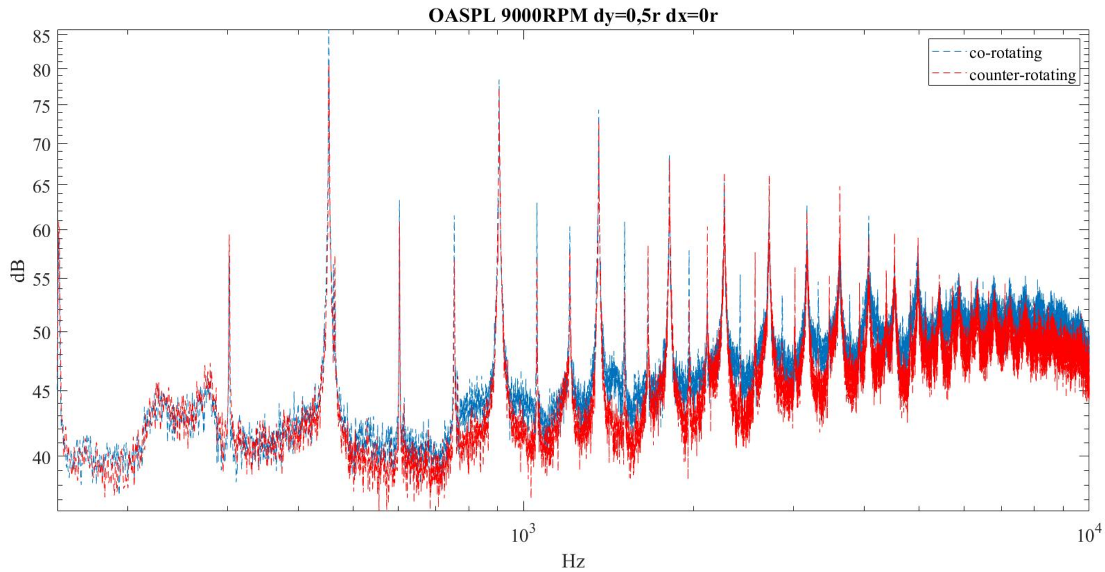


Figure 3.23: PSD $dy = 0,5r$ and $dx = 0r$ comparison between counter and co-rotating configurations.

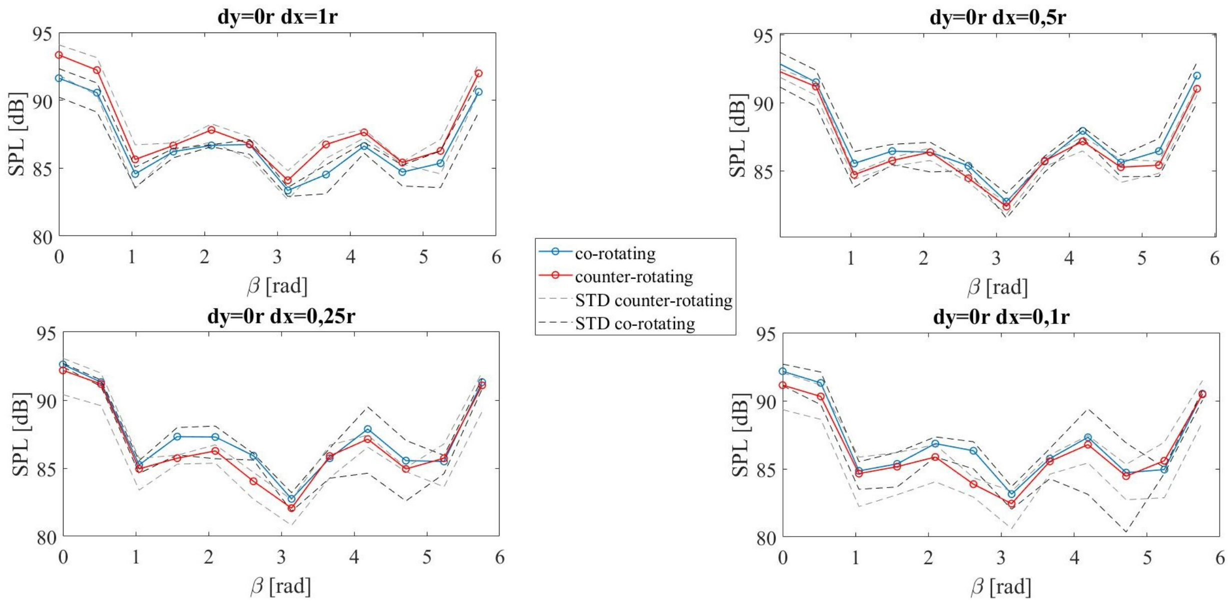


Figure 3.24: SPL co and counter-rotating comparison varying the distances with the add of a range of confidence of 95%.

### 3.0.7. Broadband Component Extraction

The broadband component can be a huge contributor to noise when the subject of interest is caught in a turbulent flow. Indeed, in the tandem propeller configuration, the back propeller is caught in the wake of the advanced one when there is overlapping of the two, moreover the wake of the propeller always interacts with its own nacelle that is a bluff body itself. Both these phenomena allow vortexes to interact with solid body creating a non-periodic broadband noise that translate into the PSD at low random fluctuations distributed over different frequencies. The broadband noise was already visible in the previous analysis of the power spectral density, indeed, to better visualise its contribution, an interpolation on the PSD has been done in order to remove the tonal peaks from the signal. All the broadband extrapolations are reported in figures 3.25, 3.26, 3.27 and 3.28 All these curves show an effective removal of the tonal peaks at low frequencies. A comparison between different broadband noise spectra at $9000RPM$ is done in figure 3.29. In general, the staggered configurations show an uniform increment in the broadband noise over all the frequencies with respect to the isolated case. Instead it is interesting to analyse the difference between the broadband noise of the staggered configuration at different distances, when the two propellers are overlapped ($dx = -0,5r$) there is an increment in the broadband of just low and mid frequencies with respect to the far opposite case of $dx = 1r$. The high-frequencies broadband noise remains almost the same for the two cases. The main contributor to broadband noise is the vortexes, and the wake is supposed to increase its turbulence decreasing the distance between the two propellers, this means that, since just the low and the mid frequencies broadband increases, the wake is composed by such turbulence frequencies oscillations. Stochastic noise can also be generated from the oscillation of RPM, since, even if the power imprinted to the engine is stable, the RPM are not fixed at one value but oscillate around an average.

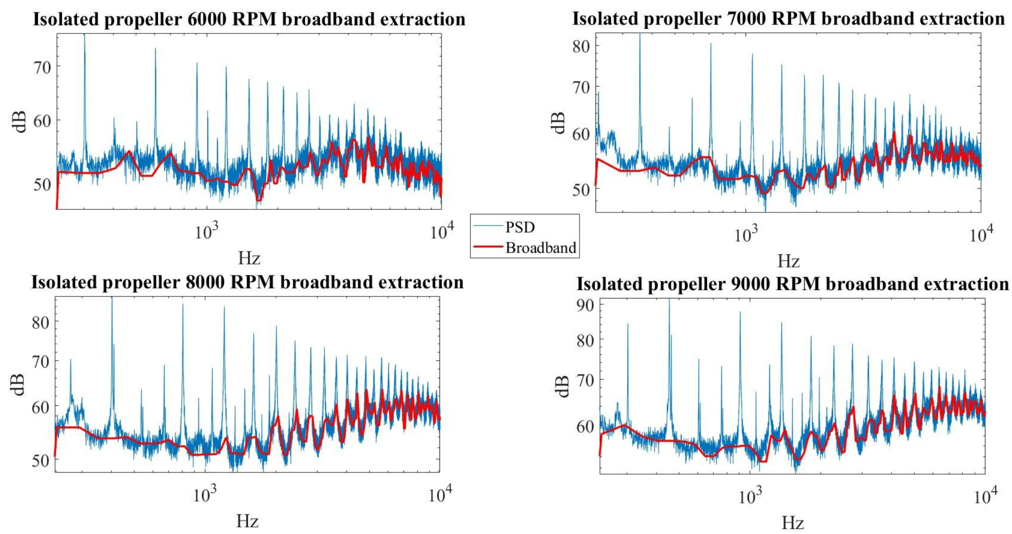


Figure 3.25: Extrapolation of the single propeller broadband noise

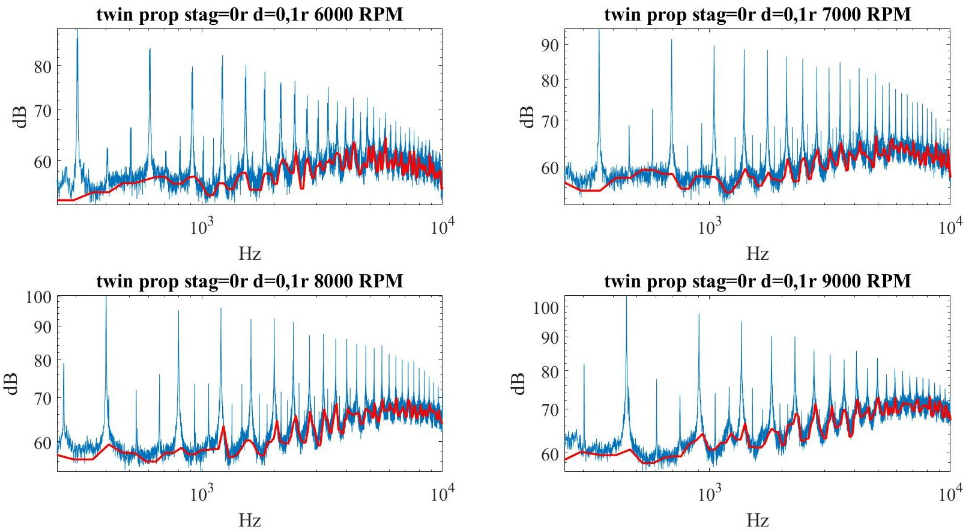


Figure 3.26: Extrapolation of the single propeller broadband noise.

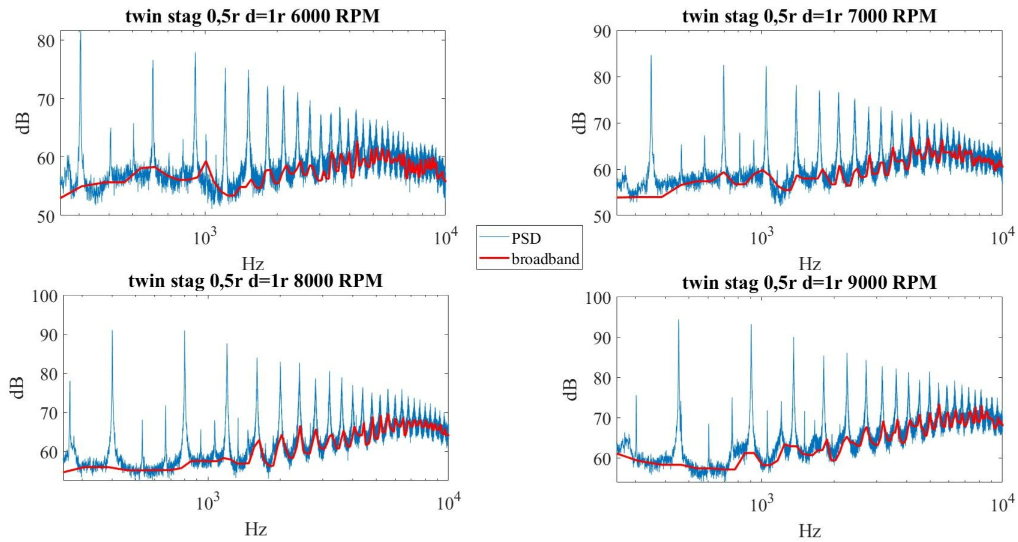


Figure 3.27: Extrapolation of the tandem propeller $dy = 0,5r$ and $dx = 1r$ broadband noise.

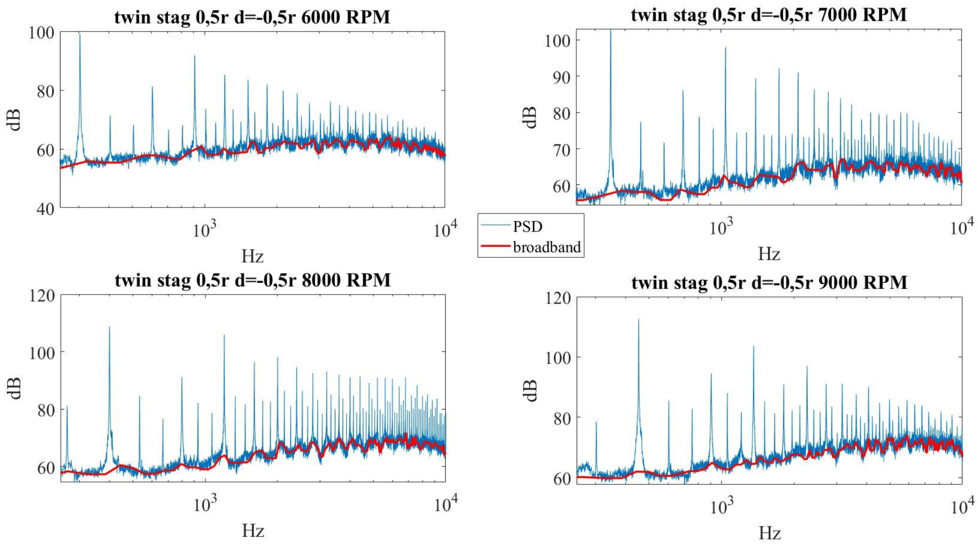


Figure 3.28: Extrapolation of the tandem propeller $dy = 0,5r$ and $dx = -0,5r$ broadband noise.

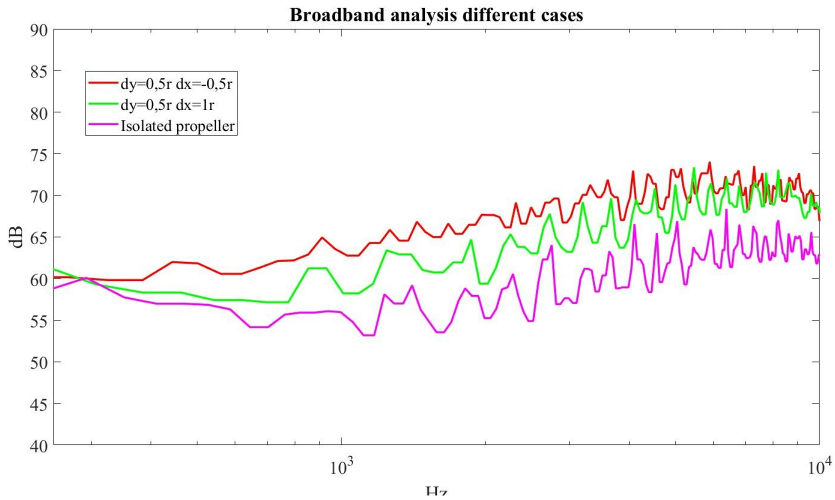


Figure 3.29: Comparison between different cases broadband noise.

### 3.0.8. A-weighted noise

In this section some of the OASPL results are going to be presented throughout A-weighting. The A-weighting consists in filtering the noise throughout an A-filter that permits to consider just the actual noise perceived by the human hearing. As a matter of fact the frequencies are not all perceived in the same way by human hear, indeed the range of frequencies in which human can hear is from $20\mu Pa$ to $20000Pa$, but, inside this range, the low frequencies until $f = 1000Hz$ are perceived as less annoying than the higher ones.

Taken this into account the it is possible to say that the OASPL is not an absolute index of the noise bothering of an aircraft, as a matter of fact if a noise has a spectrum with high peaks at low frequencies and low peaks at high frequencies could result less bothering than a noise with high peaks at high frequencies. In this case even if the area, so the OASPL, subtended at the spectrum is bigger in the first case the A-weighted OASPL would be lower in accordance with the noise perceived by the human hearing. The A-filtering consists in the mathematical addition of values at precise frequencies, in this way the low frequencies are dampened while the higher ones are amplified until $f = 10000Hz$. The A-weighting values are listed in regulations and since, throughout experience, correlation was proven with occupational deafness, it is commonly used to measure environmental noise to avoid hearing damage. The A-filter is just one curve inside a bigger family of filters, the standard that norms them is the IEC 61672:2003 (Plot in appendix B).

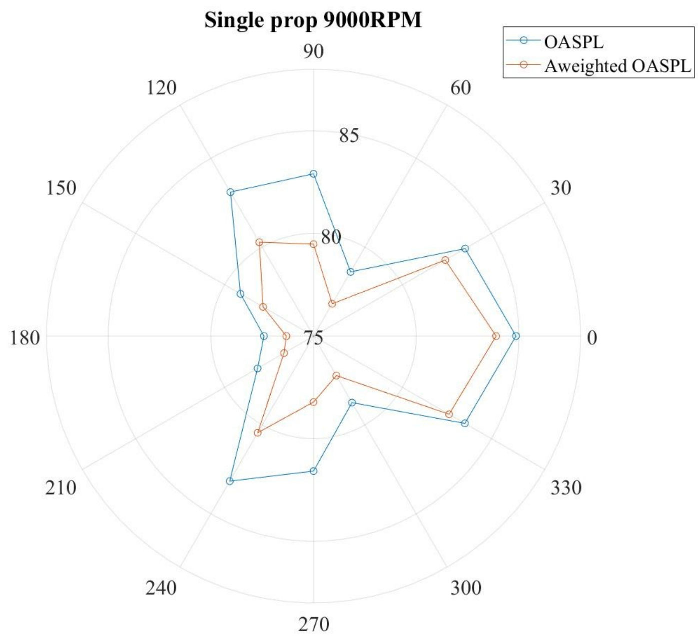


Figure 3.30: Comparison of the OASPL and the A-weighted OASPL of the isolated propeller.

As it is possible to see from the OASPL of the isolated propeller case, figure 3.30, throughout the A-weighting the noise perceived by the human hear is lower than the unweighted one, he decrement varies from $1dB$ for the microphone at $\beta = 0°$ and it is up to $3dB$ for the microphone at $\beta = 90°$.

The A-weighting filter act directly on low frequencies and high frequencies dumping them. Instead, the frequencies above $f = 1000Hz$ are slightly amplified. This behaviour is visible from figure B.1 that shows the PSD at $\beta = 90°$ for the A-weighted and unweighted isolated propeller signal.

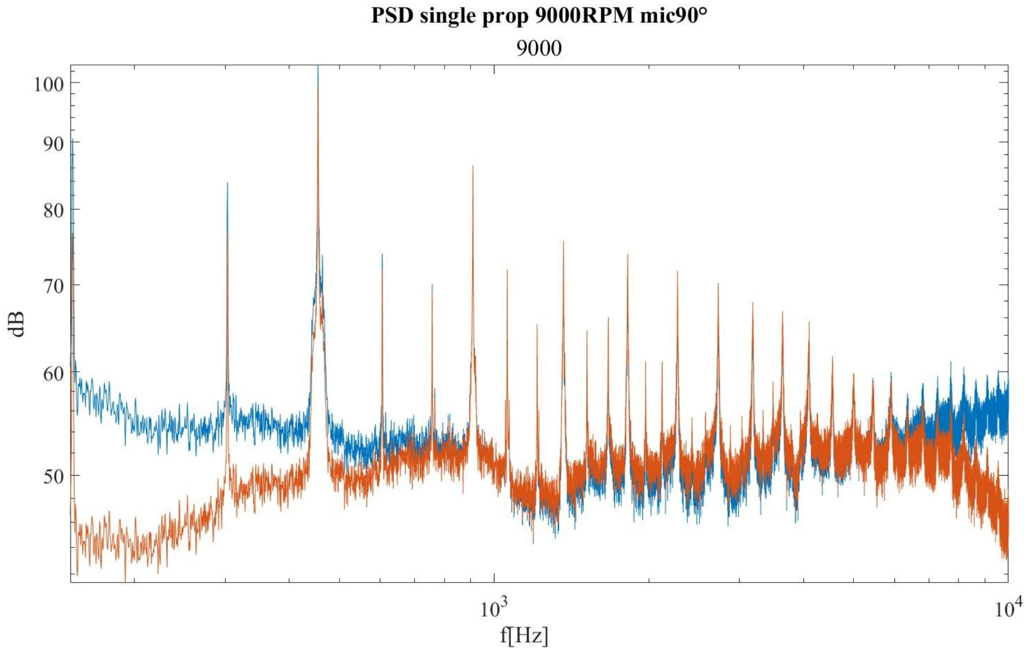


Figure 3.31: Comparison of the OASPL and the A-weighted OASPL of the isolated propeller for the 90° microphone.

In the following parts some cases of OASPL are reported in comparison with their corresponding A-weighted values. As it was shown before the tendency of the A-weighting in all the cases is to reduce the values of the OASPL, figures 3.32a, 3.32b and 3.32c. In particular decibels, with the A-weighting, is reduced more intensely toward the side of the propeller (microphones at $\beta = 90°$), this implies that the unweighted spectrum of these signals has an higher content at low frequencies that could be dampened, than the one from the microphone at $\beta = 0°$. To better visualise this phenomenon the unweighted signal for the microphones at $\beta = 0°$ and $\beta = 180°$ in the configuration of $dy = 0r$ and $dx = 0,1r$ are reported and compared in figure 3.33a and 3.33b. The high frequencies are dumped more or less in the same way, while the low frequency captured by the microphone $\beta = 90°$ are much higher and so can be dumped reducing the value of the respective OASPL.

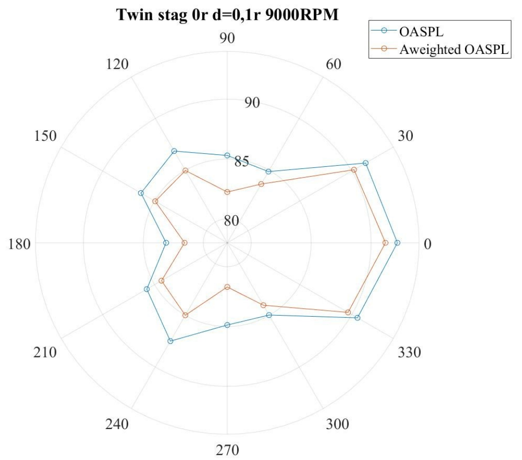


(a) Comparison of the OASPL and the A-weighted OASPL of the tandem propeller configuration with $dy = 0r$ and $dx = 0,1r$.

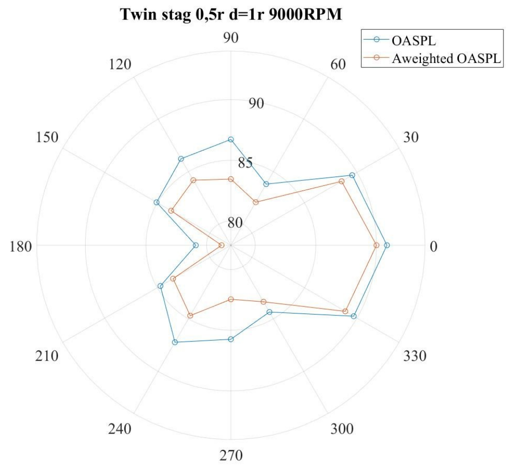


(b) Comparison of the OASPL and the A-weighted OASPL of the tandem propeller configuration with $dy = 0,5r$ and $dx = 1r$.

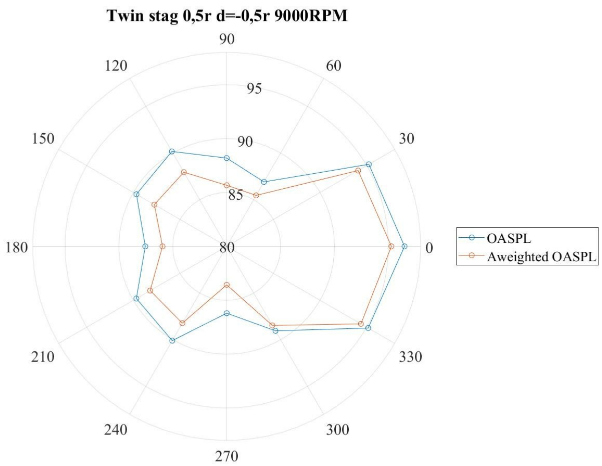


(c) Comparison of the OASPL and the A-weighted OASPL of the tandem propeller configuration with $dy = 0,5r$ and $dx = -0,5r$.

Figure 3.32: OASPL and A-weighted OASPL comparison for tandem configurations.

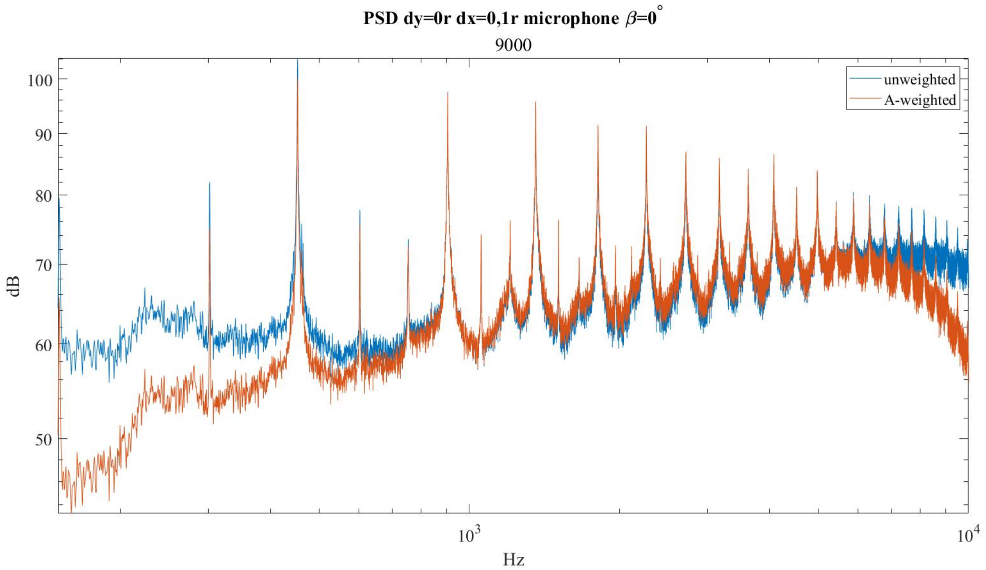


(a) PSD comparison A-weighted and unweighted signal microphone $\beta = 0°$.

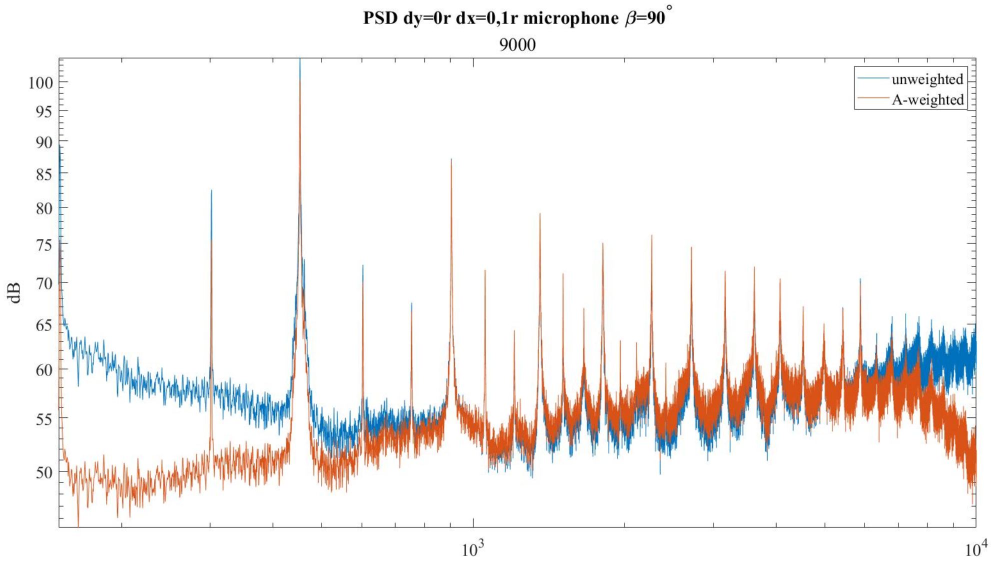


(b) PSD comparison A-weighted and unweighted signal microphone $\beta = 90°$.

Figure 3.33: PSD and A-weighted OASPL comparison.

# 4 | Chapter four
# Conclusions and Future Developments

An experimental investigation on two propellers in tandem configuration was done to deeply understand the impact on performances and acoustics of the variation of the tip-to-tip distance and the disk-to-disk distance. Moreover, since numerical tools were not used for this investigation, the numerical data set a database that can be used to validate simulation tools.
Since aeroacoustic measurements were required, the campaign was held in the anechoic chamber of the energy department at Politecnico of Milan. The chamber allows to better isolate the test area from external disturbance and to simulate a completely open environment without acoustic wave reflection on the walls, moreover also the performances measures were done in the same space. The experimental setup was designed thinking about the many possible configurations that could derive changing both the disk-to-disk value and the tip-to-tip distance, and so it was easily and fast modifiable. First of all, the isolated propeller was tested, this action allowed its characterisation from both the performances and acoustics point of view. Moreover, the obtained data were used as reference for the tandem propellers' configuration.
After this the side-by-side, tandem configuration was tested varying the tip-to-tip distance and the value of the disk-to-disk distance was varied successively. The first tests were done with the blades of the propellers co-rotating, successively also the counter-rotation was tested and its effects were verified.
These tests allow to have a complete overview on the mutual influence between two propellers in hover that could be moved in the two directions on the vertical plane:

- A mutual influence of any kind reduces the performance, in fact the reference propeller in the tandem configuration has always lower performances than the isolated one.

- The tip-to-tip distance resulted to have a relevant effect on both the performances and the noise production. As a matter of fact, when the two propellers get closer the performances are reduced while the acoustic emission increase.
- The variation of the disk-to-disk distance itself, with the tip-to-tip distance fixed, does not have a relevant impact on the performances or the acoustics. What is relevant is that the staggered configuration allows the overlapping of the disks of the propellers and so the interaction of the back propeller with the wake of the advanced one. This phenomenon brings a fall in the performance (that increases increasing the overlapping) and a remarkable increment of the noise production justified by both an intensification of the tonal peaks and the broadband noise.
- Increasing the mutual influence between the two propellers (this means both reducing the tip-to-tip distance and introducing the overlap) the thrust fluctuations increase leading to an enhancement in the tonal peaks. The peaks at low Mach speed derive from loading noise that derives from the oscillation of the forces on the blade. The oscillation of the forces, and so the tonal peaks, increase also when there is overlapping of the two propellers, the back propeller is caught in the wake of the other one and so the pitch of its blades is continuously changing bringing to a change in the forces orientation.
- Moreover, the mutual influence leads also to an increment in the turbulent kinetic energy, this phenomenon, that is particularly strong with the overlapping, brings an enhancement in the vortexes and so a remarkable increment in the broadband components of the noise in particular at low frequencies.
- Indeed the counter-rotating case, with respect to the co-rotating one, shows a slight worsening in the performances and a particular trend in the noise production. The co-rotation is the noisier for the biggest tip-to-tip distances, but when the two propellers get closer and overlap the counter-rotating one becomes the more noisy.
- It was also observed that the level in decibel has a peak of directivity in the vertical direction and slightly diminish towards the side.
- Moreover an analysis through an A-weighting filter led to the conclusion that the acoustic signal propagated laterally is composed by predominant low and mid-frequencies, this means that it bothers less the human hearing. Instead, the signal propagating vertically is characterised by more intense high frequencies, as a result it bothers more the human hearing.

## Future developments

The eVTOL's acoustic emission is still an open problem and, even if this analysis fulfilled its purpose, it still needs to be investigated. A deeper experimental investigation could be led to better understand the effects of the mutual influence of the two propellers analysing more relative distances.
The physics behind these interactions can be better understood with the visualisation of the flow and this could be done throughout different tools. A particle image velocimetry analysis could be conducted in order to instantaneously visualise the flow on different 2D planes. Instead, numerical tools enable the visualisation of the flow over time and the distribution in the domain of different flow features, for example it would be interesting to visualise the distribution of the TKE for different cases. A high-fidelity tool such as CFD method would be very precise in this purpose, but also difficult to manage due to the presence of rotating blades. A solution could be the conduction of the numerical investigation with a mid-fidelity tool such as DUST that is very suitable for the eVTOL's case. With this tool it is easy to change setting between the different configuration and to manage not stationary cases such as rotating blades. Moreover since it has been coupled to $SU^2$, the aeroacoustic performances could easily be obtained with the use of a panel method.
Moreover, since an actual eVTOL is characterised by the presence of more than two propellers, different configurations with more propellers should be studied. Furthermore, the eVTOLs take off vertically then tilt toward a forward flight configuration. These two phases could be both analysed from the acoustic and performances point of view.

# Bibliography

[1] DUST-project. `https://www.dust-project.org/`.

[2] SU2. `https://su2code.github.io/`.

[3] D. Algarotti. Experimental-numerical investigation of the aerodynamic interaction between tandem propellers in evtol airplane mode. Master's thesis, Politcnico of Milan, The address of the publisher, 7 2021.

[4] E. J. Alvarez, A. Schenk, T. Critchfield, and A. Ning. Rotor-on-rotor aeroacoustic interactions of multirotor in hover. *Journal of the American Helicopter Society*, 2020.

[5] T. Carolus, M. Schneider, and H. Reese. Axial flow fan broad-band noise and prediction. *J. Sound Vib*, 2007.

[6] S. Glegg and W. Devenport. *Aeroacoustics of low Mach number flows*. Elsevier, 2017.

[7] E. Greenwood and S. Kenneth. Challenges and opportunities for low noise electric aircraft. *International Journal of Aeroacoustics*, 2022.

[8] R. Piccinini, M. Tugnoli, and A. Zanotti. Numerical investigation of the rotor-rotor aerodynamic interaction for evtol aircraft configurations. *MDPI*, 2020.

[9] C. R. Russell and M. K. Sekula. Comprehensive analysis modeling of small-scale uas rotors. *Journal of the American Helicopter Society*, 2020.

[10] D. Thai Austin, E. De Paola, A. Di Marco, L. G. Stoica, R. Camussi, R. Tron, and S. M. Grace. Experimental and computational aeroacoustic investigation of small rotor interactions in hover. *MPDI*, 2021.

[11] M. Tugnoli, D. Montagnani, M. Syal, G. Droandi, and A. Zanotti. Mid-fidelity approach to aerodynamic simulations of unconventional vtol aircraft configurations. *Aerospace Science and Technology 115*, 2021.

[12] Y. Yang, Y. Wang, Y. Liu, H. Hu, and Z. Li. Noise reduction and aerodynamics of isolated multi-copter rotors with serrated trailing edges during forward flight. *Journal of Sound and Vibration*, 2020.

[13] N. Zawodny, B. J. Douglas, and C. L. Burley. Acoustic characterization and prediction of a representative, small-scale rotary-wing unmanned aircraft system components. *Aeroacoustics Branch, NASA Langley Research Center*.

[14] W. Zhou, Z. Ning, H. Li, and H. Hu. An experimental investigation on rotor-to-rotor interactions of small uav propellers. *Conference paper, 35th AIAA Applied Aerodynamics Conference*, 2017.

# A | Appendix A

### A.0.1. Microphones sensitivity and response in frequency

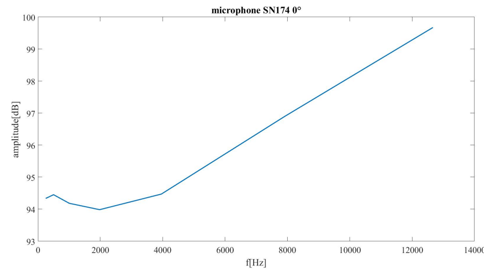


(a) Microphone SN174 positioned at $0deg$ frequency response.

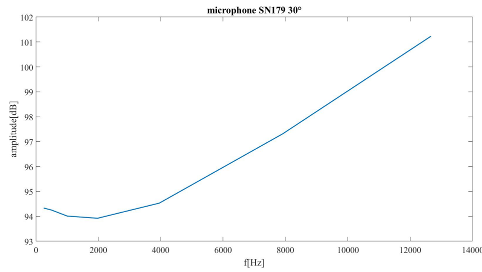


(b) Microphone SN179 positioned at $30deg$ frequency response.

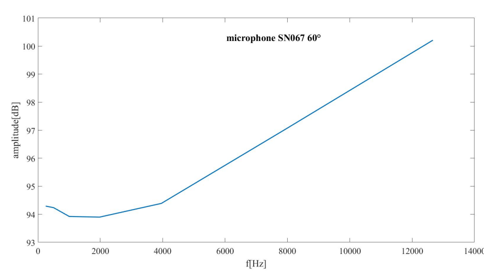


(c) Microphone SN067 positioned at $60deg$ frequency response.

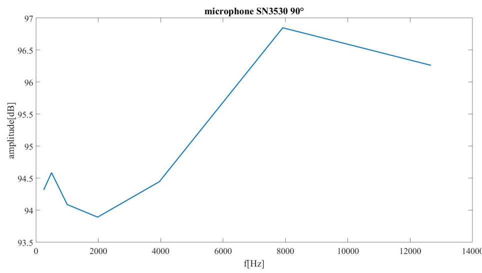


(d) icrophone SN3530 positioned at $90deg$ frequency response.

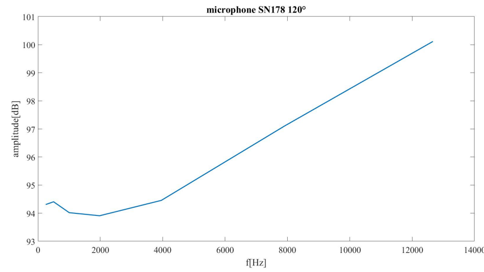


(e) Microphone SN178 positioned at $1200deg$ frequency response.

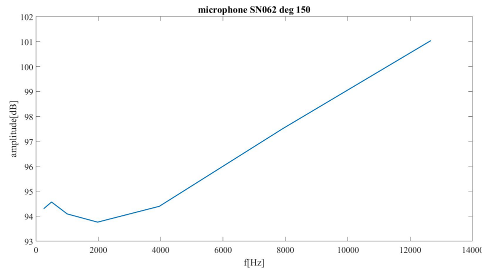


(f) Microphone SN062 positioned at $150deg$ frequency response.

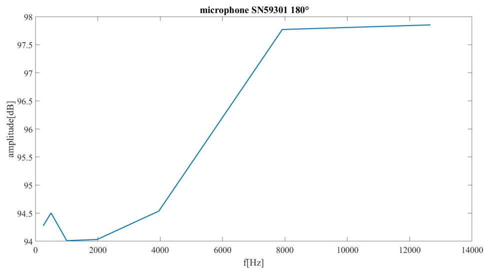


(g) Microphone SN59301 positioned at 180$deg$ frequency response.

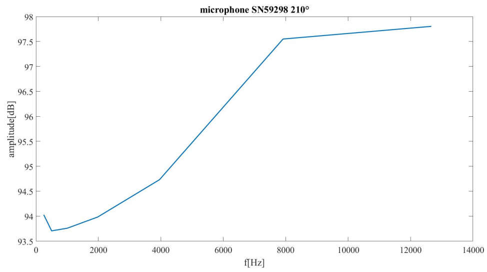


(h) Microphone SN59298 positioned at 210$deg$ frequency response.

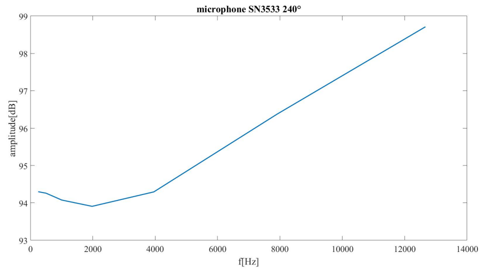


(i) Microphone SN3533 positioned at 240$deg$ frequency response.

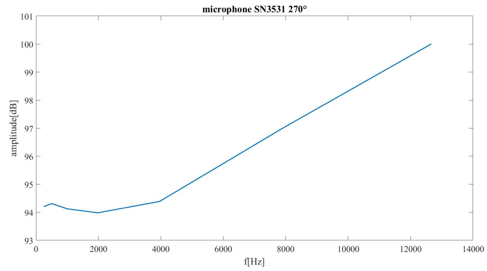


(j) Microphone SN3531 positioned at 270$deg$ frequency response.

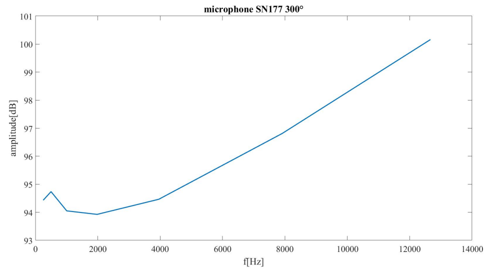


(k) Microphone SN177 positioned at 300$deg$ frequency response.

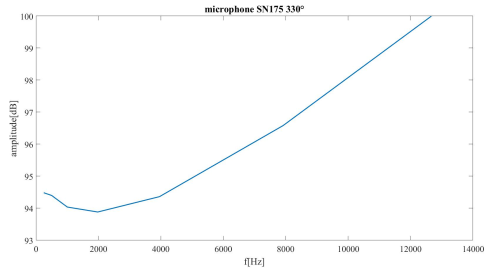


(l) Microphone SN175 positioned at 330$deg$ frequency response.

Figure A.1: Microphones sensitivity over frequency.

Moreover in the following table are reported the microphones sensitivity used.

| | **Sensitivity** $mV/Pa$ |
|---|---|
| **Mic** $\beta = 0°$ | $53,2$ |
| **Mic** $\beta = 30°$ | $39,6$ |
| **Mic** $\beta = 60°$ | $51,9$ |
| **Mic** $\beta = 90°$ | $51,2$ |
| **Mic** $\beta = 120°$ | $46,4$ |
| **Mic** $\beta = 1500°$ | $51,9$ |
| **Mic** $\beta = 180°$ | $38,5$ |
| **Mic** $\beta = 210°$ | $40,4$ |
| **Mic** $\beta = 240°$ | $52$ |
| **Mic** $\beta = 270°$ | $52,1$ |
| **Mic** $\beta = 300°$ | $53,5$ |
| **Mic** $\beta = 330°$ | $55$ |

Table A.1: Microphones sensitivity.

## A.0.2. Atmospheric Data

**day 1**

| **P** | **T** | **Ur** | |
|---|---|---|---|
| $99440Pa$ | $20,6°$ | $45,3\%$ | |
| $dy/r$ | $dx/r$ | isolated prop | |
| 0 | $1,\ 0,5,\ 0,25$ | | |

**day 2**

| **P** | **T** | **Ur** | |
|---|---|---|---|
| $99242Pa$ | $19,3°$ | $45\%$ | |
| $dy/r$ | $dx/r$ | $dy/r$ | $dx/r$ |
| 0 | $0,1$ | $0,5$ | $1,\ 0,5,\ 0,25$ |

**day 3**

| **P** | **T** | **Ur** | |
|---|---|---|---|
| $99685Pa$ | $19,6°$ | $49,6\%$ | |
| $dy/r$ | $dx/r$ | $dy/r$ | $dx/r$ |
| $0,5$ | $0,\ -0,25,\ -0,5$ | 1 | $-0,5,\ 0,\ 0,5,\ 1$ |

**day 4 Counter-rotating propellers**

| **P** | **T** | **Ur** | |
|---|---|---|---|
| $99624Pa$ | $19,1°$ | $51,2\%$ | |
| $dy/r$ | $dx/r$ | $dy/r$ | $dx/r$ |
| 0 | $0,1,\ 0,25,\ 0,5,\ 1$ | $0,5$ | $1,\ 0,5,\ 0,25,\ 0$ |

**day 5 Counter-rotating propellers**

| **P** | **T** | **Ur** |
|---|---|---|
| $100170Pa$ | $20°$ | $49,2\%$ |
| $dy/r$ | $dx/r$ | motors |
| $0,5$ | $0-,25,\ -0,5$ | |

Table A.2: Atmospheric data of the different campaign days.

# B | Appendix B

### B.0.1. A-weighted filter

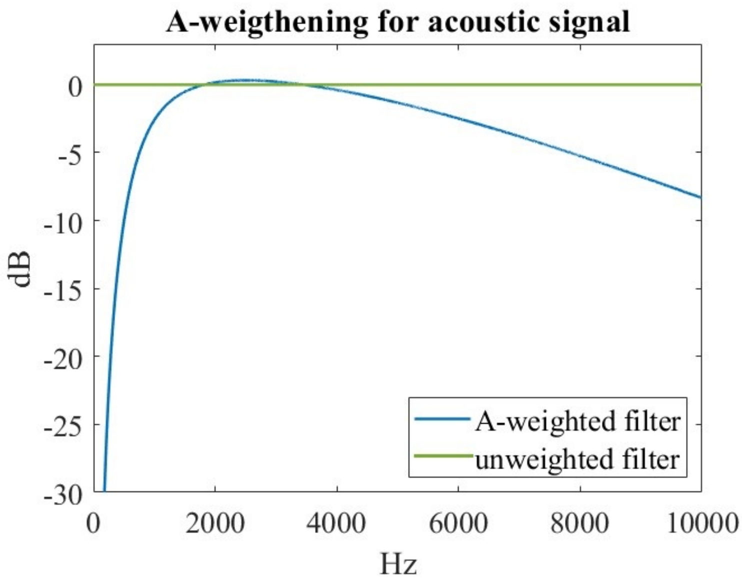


Figure B.1: Comparison between the A-weighted and the unweighted filter, plot over frequency.

# List of Figures

# List of Tables

# List of Symbols

| Variable | Description |
|---|---|
| $\alpha$ | blade pitch angle |
| $A - OASPL$ | A-weighted OASPL |
| $\beta$ | azimuthal angle |
| $BPF$ | blade passing frequency |
| $C_Q$ | torque coefficient |
| $C_T$ | thrust coefficient |
| $dx$ | tip-to-tip distance |
| $dy$ | disk-to-disk distance |
| $ESC$ | electronic speed controller |
| $f$ | frequency |
| $f_{CUT}$ | frequency |
| $f_S$ | sampling frequency |
| $G$ | microphone sensitivity |
| $h$ | half of the serration length |
| $\lambda$ | serration wave length |
| $Ma$ | Mach number |
| $N$ | number of blades |
| $OASPL$ | overall averaged sound pressure level |
| $PIV$ | particle image velocimetry |
| $PSD$ | power spectral density |
| $r$ | ray of the blade |
| $Re$ | Reynolds number |
| $RO$ | read-out |
| $RPM$ | round per minute |
| $u_\infty$ | flow self-induced velocity |

# Acknowledgements

I never thought I would arrive at this point, because five years ago I started my academic career as a mechanical engineer in Brescia. I fell in love with aeronautics and it was clear to me that this would be the path I would follow.
First of all, I would like to thank Prof. Alex Zanotti, since he made me understand and love the experimental part of this subject. He helped me with this work and also helped me with some of my future decisions. Then I would like to thank Donato Grassi and Luca Riccobene for helping me with this work and being so kind to me.
I would also like to mention Chiara Faitini for being my greatest friend, for always being there when I needed her, and for being my anchor when I lost myself. She also helped me write this paper, as she reviewed it.
These years at Politecnico of Milan may have been hard, but at least I was not alone, because Fabiana Ghilardi was always by my side, and I would like to thank her for that as well. I would also like to thank all the people I have met during these years and that have been good friends to me, because I know that they will also be with me in my next steps.
I would also like to thank my parents because they always helped me when I needed it and they never left me alone. They were always an example to me and they taught me both perseverance and humility.
Finally, I would like to remember Andrea, a friend who is no longer with me, but who was always by my side when he still could; my work is dedicated to him.

*Milano, Ottobre 2023*

*Ilaria Savoldi*